

An-Najah National University
Faculty of Graduate Studies

**A Comparative Study of the Regularization
Parameter Estimation Methods for the EEG
Inverse Problem**

By

Mohammed Jamil Aburidi

Supervisor

Dr. Adnan Salman

**This Thesis is submitted in Partial Fulfillment of the Requirements for
the Degree of Master of Advanced Computing, Faculty of Graduate
Studies, An-Najah National University - Nablus, Palestine.**

2016

**A Comparative Study of the Regularization Parameter
Estimation Methods for the EEG Inverse Problem**

By

Mohammed JamilAburidi

This thesis was defended successfully on 26 / 7 / 2016 and approved by :

Defense Committee Members

Signature

– **Dr. Adnan Salman** (Supervisor)


.....

– **Dr. Hazim Abu Sarah** (External Examiner)


.....

– **Prof. Dr. Mohammad El said** (Internal Examiner)

.....


III

Dedication

*To my mother, my father, my sisters and my brothers with respect and
love.....*

Acknowledgement

Thanks go to my supervisor Dr. Adnan Salman for his helpful and continual encouragement.

Special thanks to faculty members working in Computer science, Physics and Mathematics departments for their help and guidance.

I would also thank my family members, my parents, my sisters and my brothers for their support.

الإقرار

أنا الموقع أدناه مقدمة الرسالة التي تحمل العنوان:

**A Comparative Study of the Regularization Parameter
Estimation Methods for the EEG Inverse Problem**

أقر بأن ما اشتملت عليه هذه الرسالة إنما هو نتاج جهدي الخاص، باستثناء ما تمت الإشارة إليه
حيثما ورد، وأن هذه الرسالة ككل أو من جزء منها لم يقدم من قبل لنيل أية درجة أو بحث علمي
أو بحثي لدى أية مؤسسة تعليمية أو بحثية أخرى.

Declaration

The work provided in this thesis, unless otherwise referenced, is the
researcher's own work, and has not been submitted elsewhere for any other
degree or qualification.

Student's name:

اسم الطالب: محمد جميل أبو ربي

Signature:

التوقيع: محمد جميل أبو ربي

Date:

التاريخ: 2016-7-26

Table of Contents

No.	Contents	Page
	Dedication	iii
	Acknowledgement	iv
	Declaration	v
	List of Symbols and Abbreviations	vi
	Table of Contents	viii
	List of Tables	x
	List of Figures	xii
	Abstract	xiii
	Chapter One: Introduction	1
1.1	Source Localization Problem	1
1.2	Previous Studies	3
1.2.1	Parameter Choice Methods	5
1.2.2	The imaging approach methods	6
1.2.3	Regularization parameter	8
1.3	Objective of the Study	10
	Chapter Two: Theoretical Formulation and Methods and Materials	12
2.1	Forward Problem	13
2.2	Inverse Problem	14
2.2.1	Least Squares Method and regularization	16
2.2.2	Singular value decomposition (SVD)	18
2.2.3	Truncated singular value decomposition	20
2.2.4	Discrete Picard Condition	21
2.2.5	SVD and Tikonov Regularization	21
2.3	Methods of Choosing Regularization Parameter	22
2.3.1	L-curve Method	23
2.3.2	Generalized Cross Validation (GCV)	25
2.3.3	Normalized Cumulative Periodgram (NCP)	26
2.4	Algorithms of Solving the Inverse Problem	28
2.4.1	Minimum Norm Estimate (MNE)	28
2.4.2	Weighted Minimum Norm Estimate (WMNE)	29
2.4.3	sLORETA	30
2.4.4	eLORETA	30
2.5	Localization Error Evaluation Measures	32
	Chapter Three: Methodology	33
3.1	Introduction	34
3.2	Modeling the Human Head Electromagnetic	35

VII

3.3	The generics LFM (gLFM)	38
3.4	Sampling the Lead field Matrix	39
3.5	EEG Simulated data (Synthetic Data)	40
3.6	Tuning the regularization parameter α and solving the Inverse Problem	41
	Chapter Four: Results and Calculations	44
4.1	Discrete Picard Condition	44
4.2	The L-curve, GCV and NCP Curves	46
4.2.1	The L-curve	46
4.2.2	The GCV functional curve	49
4.2.3	NCP Curves	50
4.3	Solving the Inverse Problem	52
4.3.1	Estimating the Solution using WMNE	53
4.3.2	Solving the inverse problem using eLORETA and sLORETA	59
	Chapter Five: Conclusion	62
	References	64
	Appendix A	72
	Appendix B	77
	الملخص	ب

List of Tables

No.	Caption	Page
Table (3.1)	Tissues Parameters in 5 shells model	35
Table (3.2)	The Identification number and the coordinates of each selected dipole at the solution space	39
Table (4.1)	Comparison between the regularization parameters, the parameters obtained using L-curve, GCV and NCP methods, at different signal to noise ratios in different dipole locations, for radial orientation	40
Table A.1	Localization errors using WMNE algorithm after substituting the regularization parameter from the three methods (Lcurve, NCP and GCV). Shallow dipole is used to generate the synthetic data.	65
Table A.2	Errors using COG measure, after substituting the regularization parameter from the three methods (L-curve, NCP and GCV). Shallow dipole is used to generate the synthetic data.	66
Table A.3	Errors using Spatial Spreading measure, after substituting the regularization parameter from the three methods (L-curve, NCP and GCV). Shallow dipole is used to generate the synthetic data.	66
Table A.4	Localization errors using WMNE algorithm after substituting the regularization parameter from the three methods (L-curve, NCP and GCV). Mid dipole is used to generate the synthetic data.	67
Table A.5	Errors using COG measure, after substituting the regularization parameter from the three methods (L-curve, NCP and GCV). Mid dipole is used to generate the synthetic data.	67
Table A.6	Errors using Spatial Spreading measure, after substituting the regularization parameter from the three methods (L-curve, NCP and GCV). Mid dipole is used to generate the synthetic data.	68
Table A.7	Localization errors, after substituting the regularization parameter from the three	68

	methods (L-curve, NCP and GCV). Deep dipole is used to generate the synthetic data.	
Table A.8	Errors using COG measure, after substituting the regularization parameter from the three methods (L-curve, NCP and GCV). Deep dipole is used to generate the synthetic data.	69
Table A.9	Errors using Spatial Spreading measure, after substituting the regularization parameter from the three methods (L-curve, NCP and GCV). Deep dipole is used to generate the synthetic data.	69
Table B.1	Localization errors of eLORETA and sLORETA algorithms.	70
Table B.2	Errors using COG measure of eLORETA and sLORETA algorithms.	70
Table B.3	Spatial Spreading errors of eLORETA and sLORETA algorithms.	71

List of Figures

No.	Caption	Page
Fig.(2.1)	Three orthogonal orientations (x, y, z), red line represents the dipole moment.	13
Fig. (2.2)	Illustration of EEG source localization process	14
Fig. (3.1)	Geometric representation of the tissues of the human head (human brain, skull, human head and scalp) using MATLAB.	32
Fig. (3.2)	Generic scalp sensors (red) and 128-sampled scalp sensors (blue) (left). Sampling 64-sensors using uniformly distributed points on a unit sphere (middle). Sampling distributed dipoles at resolution of 7 mm (right) (Salman <i>et al</i> , 2014).	33
Fig. (3.3)	30 points uniformly distributed on a unit sphere, each point represents one orientation.	39
Fig. (4.1)	Discrete Picard Plots for the D3 with radial orientation at different SNR (4,8, 12 and 16). The blue dots are the singular values, the Fourier coefficients are shown in green and red circles are Fourier coefficients divided by singular values.	40
Fig. (4.2)	The L-curve for D1, D2 and D3, for two signal to noise ratios (4 and 12). The residual norm is on x-axis and solution norm on the y-axis.	40
Fig. (4.3)	The GCV functional for D1, D2 and D3 for two levels of SNR (4 and 12). The regularization parameter is on x-axis and GCV functional on the y-axis.	41
Fig. (4.4)	The NCPs for the synthetic exact (Blue line), and the NCP of the synthetic data after adding white Gaussian noise.	42
Fig. (4.5)	The NCPs curves for shallow (D1), mid (D2), deep (D3) dipoles for two levels of signal to noise ratio (from left to right). The red thick line represents the optimum NCP, which corresponds to the optimum regularization parameter.	44
Fig. (4.6)	Using WMNE algorithm, for shallow dipole , A) Show the localization error (mm) in terms	47

	of SNR after obtaining α from L-curve, GCV and NCP. B) Show distance from the center of gravity (mm) in terms of SNR. C) Show the spatial spreading (mm) in terms of SNR.	
Fig. (4.7)	Using WMNE algorithm, for mid located dipole , A) Show the localization error (mm) in terms of SNR after obtaining α from L-curve, GCV and NCP. B) Show distance from the center of gravity (mm) in terms of SNR. C) Show the spatial spreading (mm) in terms of SNR.	48
Fig. (4.8)	Using WMNE algorithm, for deep located dipole , A) Show the localization error(mm) in terms of SNR after obtaining α from L-curve, GCV and NCP. B) Show distance from the center of gravity (mm) in terms of SNR. C) Show the spatial spreading (mm) in terms of SNR.	49
Fig. (4.9)	Blue line (eLORETA), red line (sLORETA), A) Localization errors using eLORETA and sLORETA at different signal to noise ratio. B) Center of gravity errors, C) spatial spreading errors.	35

List of Symbols and Abbreviations

Φ_{EEG}	Vector of EEG potentials
K	Lead filed matrix
J	Current density vector
ϵ	Perturbation error
σ	Conductivity tensor
Γ	Tikhonov regularization constraint
α	Regularization parameter
$\ \cdot\ $	Euclidian norm
f_i	Tikhonov filter
u_i, v_i	Singular vectors of a matrix
σ_i	Singular value
κ	Curvature of the L-curve
G_α	Generalized cross validation function
P_α	Power spectrum
W_i	Weighted matrix

**A Comparison Study of the Regularization Parameter Estimation
Methods for the EEG Inverse Problem**

By

Mohammed Jamil Aburidi

Supervisor

Dr. Adnan Salman

Abstract

Investigation of the functional neuronal activity in the human brain depends on the localization of Electroencephalographic (EEG) signals to their cortex sources, which requires solving the source localization inverse problem. The problem is ill-conditioned and under-determinate, and so it is ill-posed. To find a treatment of the ill-posed nature of the problem, a regularization scheme must be applied. A crucial issue in the application of any regularization scheme, in any domain, is the optimal selection of the regularization parameter. The selected regularization parameter has to find an optimal tradeoff between the data fitting term and the amount of regularization.

Several methods exist for finding an optimal estimate of the regularization parameter of the ill-posed problems in general. In this thesis, we investigated three popular methods and applied them to the source localization problem. These methods are: L-curve, Normalized Cumulative Periodogram (NCP), and the Generalized-Cross Validation (GCV). Then we compared the performance of these methods in terms of accuracy and

reliability. We opted the WMNE algorithm to solve the EEG inverse problem with the application of different noise levels and different simulated source generators. The forward solution, which maps the current source generators inside the brain to scalp potential, was computed using an efficient accurate Finite Difference Method (FDM) forward solver. Our results indicate that NCP method gives the best estimation for the regularization parameter in general. However, for some levels of noise, GCV method has similar performance. In contrast, both NCP and GCV methods outperforms the L-curve method and resulted in a better average localization error.

Moreover, we compared the performance of two inverse solver algorithms, eLORETA and sLORETA. Our results indicate that eLORETA outperform sLORETA in all localization error measures that we used, which includes, the center of gravity and the spatial spreading.

Chapter One

Introduction

1.1 Source Localization Problem

In neuroscience, the accuracy of brain imaging techniques like electroencephalography (EEG) (Grechet *et al*, 2008) and magnetoencephalography (MEG) (Uitert *et al*, 2003), require solving, what is called, *the source localization problem*. The source localization problem is the problem of inferring an estimate of the brain current sources that generates the electric potentials on the scalp and the magnetic field near the scalp. These fields are measured using recording sensors technologies (Tucker, 1993). Electromagnetic-based (EM) imaging techniques like EEG and MEG provide direct measurement of the neural activity in the range of milliseconds temporal resolution. However, due to the ill-posed nature of the neuroscience source localization problem and the volume conduction characteristics of the human head, the spatial resolution is limited to few centimeters. In contrast, indirect imaging modality such as functional Magnetic Resonance Imaging (fMRI) (Liu *et al*, 1998) and Positron Imaging Tomography (PET) (Cherry *et al*, 1996), provide indirect measurements of brain spatiotemporal activity in the range of seconds temporal resolution and millimeter spatial resolution. Therefore, improving the spatial resolution of EM based imaging will allow achieving a high spatiotemporal brain functional imaging.

Two approaches are used in solving the source localization problem: 1) the equivalent dipole model, and 2) the distributed dipole model. The equivalent dipole model is based on the assumption that the scalp EEG signal is generated by one or few current dipoles, whose locations and moments are to be determined using a nonlinear search algorithm (Fender, 1987 and Scherg *et. al*, 1985). The drawback of this approach is the required specification of the number of dipoles. Underestimating them causes biased results by the missing dipoles. Overestimating them, causes the dipoles to fit any data. In the distributed model approach, the primary current sources are assumed to be current dipoles distributed inside the brain. The number of dipoles must be large enough ($\sim 2,000 - 10,000$) to cover the cortex with an optimal resolution. Then, the potentials due to these dipoles at the scalp electrodes is computed using the forward solver of Poisson equation to obtain a lead field matrix (LFM), which provide the linear relationship between the current dipoles and the potentials at the scalp electrodes, $\Phi = KJ + \epsilon$. Then, the goal of the source localization problem is to invert the forward equation to find an estimate of the current sources J , given the LFM K and scalp measurements Φ_{EEG} .

However, since the LFM K is 1) ill-condition (has high condition number), which causes a highly-sensitive solutions to noise and 2) underdetermined, where the number of dipoles (columns) is much higher than the number of electrodes (rows), which means the solution is not unique and there is an infinitely many solutions that would explain a given EEG signal. One approach to find a unique and stable solution is to apply a regularization

scheme. In this approach the inverse solution is approximated by a family of stable solutions. However, these regularization schemes involve a *regularization parameter* α that controls a tradeoff between the stability of the solution and the goodness of the fit to the data. Overestimating α , results in a stable solution, but bad fit to the data. Underestimating α , causes a good fit to the data, but unstable solution. Therefore, tuning and finding the optimal value of α is crucial to the quality and stability of the solution. In the literature, there exist several methods for tuning the regularization parameter includes: L-curve (Hansen, 1993 and Hansen, 1994), Normalized Cumulative Periodogram (NCP) (Hansen, 2006 and Hansen, 2007), and the Generalized-Cross Validation (GCV) (Wahba, 1977 and Golub, 1979). However, the quality of each method is likely depends on the characteristic of the particular inverse problem. In this thesis, we investigated the quality of these methods in tuning the regularization parameter for neuroscience source localization problem. We compared their performance and the quality of the inverse solution using three measures of error, localization error, center of gravity, and spatial spreading.

1.2 Previous Studies

Non-invasive brain imaging techniques such as MEG, EEG, fMRI and PET allow researchers and physicians to explore the brain functional activities and problems without invasive neurosurgery. These techniques has many important applications in several domains including cognitive neuroscience

(Srinivasan, 2007), psychology (Klimesch, 1996), and medicine (Min and Luo, 2009).

A high spatiotemporal resolution of these techniques in the range of millimeter and milliseconds is necessary in most applications. However, the spatiotemporal resolution depends on the underlying process used in each technique. MEG and EEG are based on the electromagnetic signal induced by the activated regions in the cortex and measured on the scalp. Therefore, these techniques typically have a high temporal resolution. In contrast, fMRI and PET are based on hemodynamic changes and metabolism processes of the brain active regions (Liu *et al*, 1998; Cherry *et al*, 1996), respectively. Consequently, their temporal resolution is poor. In this thesis our focus is on the EEG imaging modality due to its reliability, low cost, and comfort to the subject.

EEG is a neuroimaging technique was first developed by Hans Berger in 1924 (Tudor *et al*, 2005). It provides direct measurements for the neural activity in the range of milliseconds temporal resolution, but with low spatial resolution in the range of centimeters. It has been used to diagnose different neural disorders such as epilepsy and tumors.

Considerable efforts have been made in order to improve the spatial resolution of EEG modality throughout the years. Nunez (Nunez *et al*, 1994) and Sidman (Sidman *et al.*, 1991) developed two distinct methods to estimate the cortical surface potentials from the scalp potential. Further,

Law and others (Law *et al.*, 1993, Srinivasan *et al.* 1996, Babiloni *et al.*, 1996) presented a method to estimate the cortical surface Laplacians.

Several methods have been developed to solve and improve the spatial resolution of the source localization problem. Most of these methods are based on two approaches, the parameter approach (or the equivalent dipole methods), and the imaging approach (the distributed dipole methods). A comprehensive survey of these and other methods can be found in (Darvas *et al.*, 2004; Baillet and Mosher, 2001).

1.2.1 Parameter approach methods

The parametric approach uses the equivalent dipole model to represent a focal brain activity. In this model, multiple equivalent dipoles are used to model multiple active brain regions. The model is based on the assumption that the scalp EEG signal is generated by one or few equivalent dipoles whose locations and moments (six parameters for each dipole) are unknown (Fender, 1987; Scherg *et. al.*, 1985). The number of equivalent dipoles can't exceed the number of measuring electrodes. Then, an estimate of these parameters are obtained by minimizing the objective function,

$$E(r_{qi}, d_{qi}) = \|\Phi_{EEG}(r) - \Phi_{model}(r, r_{qi}, d_{qi})\|^2 \quad (1.1)$$

where: $\Phi(r, r_{qi}, d_{qi})$ is the electric potential at sensor location r corresponding to a current dipole d_{qi} located at r_{qi} . The electric potentials at the sensors can be computed using a certain forward model. Additional constraints on the estimated number of dipoles, which parameters are fixed,

and whether to consider the time-series of the EEG data are generally applied (Frank, 1952; Rush and Driscoll, 1968).

The main difficulty of this approach is in finding an optimal estimate of the number of dipoles. Overestimating their number causes the dipoles to fit any data and requires intensive computation due to increasing dimensionality. Underestimating their number, results in a biased solution by the missing dipoles. The accuracy of predicting the number of dipoles is questionable.

1.2.2 The imaging approach methods

The distributed dipole methods (imaging approach) are developed to overcome the requirement of identifying the optimal number of dipoles in the parametric approach. In these methods, a large number of current dipoles are distributed inside the brain. Since the position of each dipole is a potential location of a current source associated with a brain activity, the number of dipoles must be large enough to cover the brain with an optimal resolution. The electric potential due to each dipole at the scalp electrodes are then calculated using the forward solution to form a lead field matrix (LFM) K . The LFM K maps the current dipole generators inside the brain to the electric potential at the scalp electrodes in what is called the forward equation,

$$\Phi = KJ + \varepsilon, \quad (1.2)$$

where Φ is the electric potentials at the scalp electrodes, J is the current density at each dipole, and ε is noise. Then, for a given EEG data Φ_{EEG} the goal of the inverse problem is to invert the forward equation to find an estimate of the current density \hat{J} at each dipole location. Unfortunately, the problem is underdetermined and there exist an infinite number of different current configurations that would explain a given EEG data. Further, the problem is ill-conditioned, which results in an unstable solution in the presence of noise. Therefore, the problem is ill-posed. To overcome the first issue, methods impose a priori constraints on the solution to select a unique solution. To find a treatment for the second issue, methods take regularization schemes into account.

In the literature several inverse methods with different techniques and algorithms were developed. Hämäläinen and Ilmoniemi introduced the minimum norm estimate (MNE) (Hämäläinen and Ilmoniemi, 1984), which is the first discrete approach to solve the MEG inverse problem. MNE approach uses the least-squares method to determine the current dipoles that induce the scalp signals. However, solutions obtained using the MNE method is biased toward the superficial sources. Further, the method failed to handle deep current sources.

In order to overcome the preference of the superficial sources in the MNE method, Lin and his group proposed the weighted minimum norm estimate (WMNE) (Lin et al, 2006). The WMNE compensates for the bias of MNEs of favoring weak and surface sources.

Low resolution brain electromagnetic tomography (LORETA) is an algorithm presented by Pascual-Marquis and his team to estimate a good accuracy of source localization, by achieving the smallest 2nd derivatives of the current density distribution (Pascual-Marqui et al, 1994).

Pascual-Marquis developed another minimum norm approach with zero localization error and with a location wise weighting, unlike the method introduced by Dale (Dale et al, 2000), which has systematic non-zero localization. The method is called Standardized low resolution brain electromagnetic tomography (sLORETA) (Pascual-Marqui, 2002). It based on images of standardized current density (Pascual-Marqui, 1999).

Another powerful algorithm based on recursive, weighted minimum norm estimate has been developed to treat the EEG inverse problem by Gorodnitsky and his group (Gorodnitsky et al, 1995). Termed FOCUSS (FOCal Underdetermined System Solution).

Shrunked Loreta-FOCUSS (sLOFO) by Liu (Liu et al, 2004), Standardized Shrunked Loreta-FOCUSS (ssLOFO) by (Schimpf et al, 2004) and sLORETA-FOCUSS by Khemakhem and his team (Khemakhem et al, 2008) are different algorithms treat the source reconstruction inverse problem.

1.2.3 Regularization parameter

A crucial issue in the application of any regularization scheme, in any domain, is the optimal selection of the regularization parameter. Several

methods have been developed to automatically tune it. A well known method, called the discrepancy principle, (Morozov, 1966) is based on a priori knowledge about the upper bound on the noise level. Unfortunately, the method is highly sensitive to the upper bound estimation on noise.

Later on, Hansen proposed the L-curve criterion (Hansen et al, 1993 and Hansen, 1994) that do not require a priori estimate on the noise. The L-curve method is based on a log-log plot of the norm of a regularized term versus the data fitting term. The idea is that the regularization parameter corresponds to the corner of the curve, where it provides a good balance between the two norms. The corner can be obtained by calculating the curve curvature (Hansen, 2001).

A more recent method called the U-curve (Krawczyk-Stando and Rudnicki, 2007; Krawczyk-Stando and Rudnicki, 2008) is based on a plot of the sum of the reciprocals of the regularized solution norm and the residual norm. U-curve criterion selects the regularization parameter according to the maximum curvature close to the left vertical part of the U-curve.

Another popular method that doesn't require an upper bound on the noise is the Generalized cross-validation (GCV) (Golub et al, 1979 and Wahba, 1977). The method considers a statistical approach that seeks to minimize the predictive mean-square error. The GCV method works with the GCV function in finding the regularization parameter that archives the minimum value of the function.

Another statistically-based method, called normalized cumulative periodogram (NCP) (Hansen et al, 2006) was developed recently. The method tries to find a regularization parameter that can acquire the most amount of information from the residual vector. NCP chooses the regularization parameter that make the residual vector resemble the white Gaussian noise vector. This method is based on the power spectrum of the residual vector and it uses the Fourier transform in its procedures.

Further, Bazan (Bazani, 2008) proposed the Fixed-point iterations method based on the zero crossing method (Gulrajani and Johnston, 1997; Gulrajani and Johnston, 2006). Johnston and Gulrajani use zero crossing method to determine a regularization parameter of the inverse problem of electrocardiography.

Ventouras and his team studied the minimum product criterion to determine the Tikhonov regularization parameter in real evoked potentials data inversions of MEG inverse model (Ventouras et al, 2001), when the amount of noise present in the measured data is unknown.

1.3 Objectives of the Study

The main goal of this study is to improve the spatial resolution of the source localization problem for EEG source imaging under noise by finding the optimal method for regularization parameter estimation. To achieve this goal, the study will conduct the following:

- 1) Estimation of the regularization parameter using L-curve, NCP and GCV methods. We will apply these methods using different levels of white Gaussian noise, and using several test dipole's positions and orientations.
- 2) Application of the WMNE algorithm to solve the EEG inverse problem using the estimated regularization parameter by the above methods.
- 3) Evaluation of the localization error and the focus of the solution according to three measures, distant to the dipole with maximum estimated current, center of gravity, and spatial spreading.
- 4) A comparison study between these methods according to the quality of the solution and the performance.

Chapter Two

Theoretical Formulation and Methods and Materials

The general aim of electroencephalogram (EEG) source localization is to estimate the brain activity from given EEG data that arise by electromagnetic sources; it consists of solving forward and inverse problems. The forward problem is to compute the electric potential on the scalp for a given current dipole source inside a brain, Section 2.1: show information about forward problem. Inverse problem is to estimate the current sources inside the brain for a given electric potential. Several algorithms are existed to solve the inverse problem; the inverse problem is discussed in details in section 2.2. In this section, we also introduce some mathematical concepts which are important to well understand the inverse problem, these techniques are: least squares method and regularization, singular value decomposition, truncated singular value decomposition, Discrete Picard Condition and Tikhonov regularization. Methods of choosing the regularization parameter are discussed in section 2.3, mathematical details of three regularization parameter methods (L-curve, NCP, and GCV) have been illustrated in this section. Section 2.4 illustrates some of the inverse problem algorithms, which are MNE, WMNE, sLORETA and eLORETA. Finally, in section 2.6: we present three error measures are used as an evaluation tools for the perfectness of the inverse problem solution.

2.1 Forward Problem

In response to external stimuli, thousands or tens of thousands of arranged neurons are activated in a way that their induced current adds up. This net current is strong enough to propagate through the head tissues to the scalp where it can be measured using EEG sensors. These current generators are well accepted to be modeled as current dipole sources, because the measuring sensors are far away from the current source region. Computing the electric potential on the scalp for a given current dipole source inside a brain is a well-defined problem, called the EEG forward problem (Rubio and Troparevsky, 2006). Formally, it can be stated as follows: Given a volume conductor with boundary Ω , current sources within the volume induce electric and magnetic fields which can be calculated on the surface. If the conductivities σ and the current sources S are known, the electric and magnetic fields inside the volume are fully described by the quasi-static approximation of Maxwell's equations—Poisson equation (Hämäläinen *et al.*, 1993),

$$\nabla \cdot (\sigma \nabla \Phi) = S, \quad (2.1)$$

in Ω , with no-flux Neumann boundary conditions on the scalp,

$$\sigma(\nabla \Phi) \cdot n = 0, \quad (2.2)$$

where σ is the conductivity tensor, Φ is the potential, S is the current source, and n is the normal to the surface boundary. The solution of Equation (2.1) depends on the volume conduction properties, geometry and conductivity

and its solution can be obtained using numerical methods such as Finite Difference Method (FDM) and Finite Element Method (FEM). In this thesis, we used a FDM solver that we already have (Hallez H *et al*, 2005).

2.2 Inverse Problem

Several approaches are used to solve the source localization inverse problem (Darvas F *et al*, 2004; Baillet S, 2001; Pascual-Marqui R, 1999). But, in this thesis, we only consider models based on the distributed dipole approach. In this approach, the brain is covered with a large number of dipoles N ($N \sim 5,000 - 10,000$). Then the electrical potential due to each dipole at the scalp electrodes, called the *lead field* (the potential at $M \sim 32 - 512$ scalp electrodes) is computed using the forward solver for the three orthogonal orientations of the dipole moment, x , y , and z .

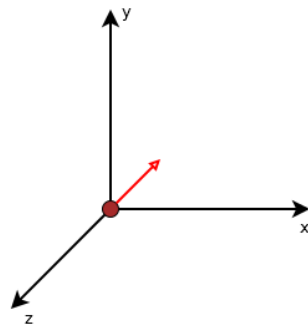


Fig. (2.1): Three orthogonal orientations (x , y , z), red line represents the dipole moment.

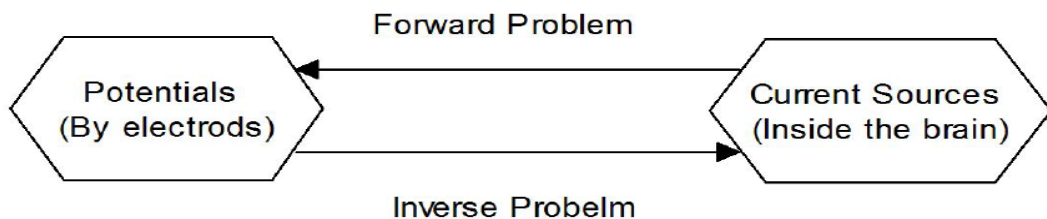


Fig. (2.2): illustration of EEG source localization process

The resulted matrix of the lead fields is called the *field matrix* K , and it has the dimension of $M \times 3N$. The lead field matrix defines the relationship between the dipole current density J and the electric potentials at the scalp electrodes Φ , in what is called, the *forward linear equation*,

$$\Phi = KJ + \epsilon, \quad (2.3)$$

where $K \in \mathbb{R}^{M \times 3N}$ is the Lead Field matrix with three coordinates for each current dipole, each element in K represents the electric potential due its current source, $J \in \mathbb{R}^{3N \times 1}$ is the primary current density vectors, ϵ is a perturbation error, and $\Phi \in \mathbb{R}^{M \times 1}$ is a vector containing scalp electric potentials measured at M sensors. Every row in K is a lead field corresponding to a current dipole obtained by solving the forward problem.

The goal of the inverse problem is to invert Equation (2.3) to find an estimate of the current densities column vector \hat{J} .

The lead field matrix (LFM) $K \in \mathbb{R}^{M \times 3N}$ is a matrix with three coordinates for each current dipole, each element in K represents the electric potential due its current source. The LFM K has the following structure:

$$\begin{bmatrix} k_{1,1} & \cdots & k_{1,N} \\ \vdots & \ddots & \vdots \\ k_{M,1} & \cdots & k_{M,N} \end{bmatrix}$$

With $k_{i,l} \in \mathbb{R}^{1 \times 3}$, for $i = 1, \dots, M$, and for $l = 1, \dots, N$. Note that $k_{i,l} = (k_{i,l}^x, k_{i,l}^y, k_{i,l}^z)$. Where the $k_{i,l}^x$ is the scalp electric potential at the i^{th} electrode.

2.2.1 Least squares method and regularization

In this section we review the methods used to solve the source localization ill-posed problem based on the distributed dipole model. The goal of the inverse problem is to invert the forward equation,

$$KJ = \Phi \quad (2.4)$$

To find an estimate for the current sources J that best explain a given EEG data Φ_{EEG} . The standard approach is to use the ordinary least square method seeking to minimize the sum of the squared residuals, $\|KJ - \Phi\|^2$. However, in this case, the linear system is ill-posed where a unique and stable solution does not exist. Two issues must be addressed in finding a useful solution for the problem.

- 1) The system is underdetermined, since the number of unknowns (the locations and orientations of the distributed dipoles is in the range of thousands) is significantly larger than the number of constraints (the number of electrodes in the range of hundreds).
- 2) The system is ill-conditioned, since a small perturbation in the right hand side Φ_{EEG} due to noise or a small perturbation to the coefficient matrix K would result in a large change in the solution.

To address these issues, a regularization term is added in order to give a preference to a particular solution with some desirable properties, and also to improve the conditioning of the problem and obtain a unique and stable

solution. Then instead of minimizing the sum of the squared residuals only, a regularization term is added, and the problem become to minimize,

$$f_{\alpha}(J) = \|KJ - \Phi_{EEG}\|^2 + \alpha \|\Gamma J\|^2, \quad (2.5)$$

Where $\|\Gamma J\|^2$ is the constraints and regularization term, $\|KJ - \Phi_{EEG}\|^2$ is the data fitting term or residual norm, and α is the regularization parameter. The regularization parameter α must find a good compromise between the two norms in order to minimize the error in the regularized solution. Overestimating α results in a stable solution but a bad fit to the data. Underestimating α results in a good fit to the data, but unstable solution.

The difference between different source localization methods that apply regularization scheme is in the constraints Γ that they apply. In this thesis, we consider the MNE (Hamalainen1984), method where $\Gamma = I$ (which corresponds to Tikhonov regularization scheme (Tikhonov,1963)), and the weighted minimum norm (WMNE), where $\Gamma = R$, is a weighting matrix. Other constraints are used in the literature, for instance, in LORETA, they used $\Gamma = \nabla$, to enforce smoothness of the current generators.

In case of MNE and WMNE, Γ is independent of J , then, the solution of Equation (2.5) can be found by differentiating the equation with respect to J and then setting the derivative to zero.

$$\begin{aligned}
f_\alpha(J) &= \|KJ - \Phi_{EEG}\|^2 + \alpha \|\Gamma J\|^2 \\
&= (KJ - \Phi_{EEG})^T (KJ - \Phi_{EEG}) + \alpha (\Gamma J)^T (\Gamma J) \\
&= J^T K^T KJ - J^T K^T \Phi_{EEG} - \Phi_{EEG}^T KJ + \Phi_{EEG}^T \Phi_{EEG} + \alpha J^T \Gamma^T \Gamma J
\end{aligned} \tag{2.6}$$

Differentiating Equation (2.6) with respect to J , and using the fact $\frac{\partial(x^T Ax)}{\partial x} = 2A$, $\frac{\partial(x^T A)}{\partial x} = A$, also, noticing that the third term is just the transpose of the second term and both terms are scalars, so their derivative is the same,

$$0 = 2K^T KJ - 2K^T \Phi_{EEG} + 2\alpha \Gamma^T \Gamma J$$

Solving for J , we get

$$J = (K^T K + \alpha \Gamma^T \Gamma)^{-1} K^T \Phi_{EEG} \tag{2.7}$$

Notice that, if $\Gamma = 0$, the solution becomes that corresponds to the ordinary least square solution.

$$J = (K^T K)^{-1} K^T \Phi_{EEG}$$

2.2.2 Singular value decomposition

The case of Tikhonov regularization when $\Gamma = I$, can be analyzed further to give more insight about the structure and conditioning of the problem via the singular value decomposition. The singular value decomposition (SVD) of a matrix K with dimension $m \times n$ is,

$$K = U\Sigma V^T = \sum_{i=1}^m u_i \sigma_i v_i^T \quad (2.10)$$

The SVD decomposition has the following properties.

1. $U^T U = V^T V = I$
2. $U \in R^{m \times m}$ and $V \in R^{n \times n}$
3. The dimension of Σ is the same as the dimension of K
4. If $m < n$, the matrix Σ is

$$\Sigma = \begin{pmatrix} \sigma_1 & 0 & \cdots & 0 & \cdots & 0 \\ 0 & \sigma_2 & \cdots & 0 & \cdots & \vdots \\ \vdots & \vdots & \ddots & \vdots & \cdots & \vdots \\ 0 & 0 & \cdots & \sigma_m & \cdots & 0 \end{pmatrix}$$

And $\sigma_1 \geq \sigma_2 \geq \cdots \geq \sigma_N$ the diagonal elements of Σ are called the singular values of K . The columns of U are the left singular vectors and the columns of V are the right singular vectors.

5. The orthonormal set of vectors V are mapped by the matrix K into the orthonormal set of vectors U , and the orthonormal set of vectors U are mapped by the matrix K^T into the orthonormal set of vectors V ,

$$\begin{aligned} KV &= (U\Sigma V^T)V = (U\Sigma)V^T V = U\Sigma \\ K^T U &= (V\Sigma^T U^T)U = (V\Sigma^T)U^T U = V\Sigma^T \end{aligned}$$

(2.11)

6. Since the singular values are $\sigma_1 \geq \cdots \geq \sigma_r \geq \sigma_{r+1} = 0 = \cdots = \sigma_m$ ($m < n$), it follows that $\text{rank}(K) = r$, and the vectors $u_i = (u_1 \ \cdots \ u_n)$ from the range of K and the vectors of $v_i = (v_1 \ \cdots \ v_n)$ from the range of K^T . Also, the vectors of

$u_i = (u_1 \ \cdots \ u_n)$ from the Null space of K , while the vectors $v_i = (v_1 \ \cdots \ v_n)$ from the null space of K^T .

7. The condition number of the matrix K is, $cond = \frac{\sigma_1}{\sigma_N}$. Since $\sigma_1 \gg \sigma_N$, the condition number is large and the problem is ill conditioned. Therefore, in terms of SVD decomposition, we can write the solution of the linear system $Kx = b$, as

$$\begin{aligned}
 U\Sigma V^T x &= b \\
 x &= (U\Sigma U^T)^{-1}b \\
 &= V\Sigma^T U^T b \\
 &= \sum_i \frac{u_i^T b}{\sigma_i} v_i
 \end{aligned} \tag{2.12}$$

Here, we see that the singular values decay toward zero and that small value cause the instability in the solution.

2.2.3 Truncated SVD Decomposition (TSVD)

The SVD solution x obtained in Equation (2.12) can be used to obtain a method for computing a regularized approximate solution. The idea is to filter out those SVD components that are dominated by noise (those components with small singular values). The resulted methods is the Truncated SVD (TSVD)

$$x_k = \sum_{i=1}^k \frac{u_i^T b}{\sigma_i} v_i, \quad k < N, \tag{2.13}$$

where k is the truncation parameter. The idea is hopefully to damp the contribution from the errors in the right hand side. Thus, the TSVD of the matrix A is defined as the rank- k matrix,

$$A_k = U \Sigma_k V^T = \sum_{i=1}^k u_i \sigma_i v_i^T, \text{ where, } \Sigma_k = \text{diag}(\sigma_1, \dots, \sigma_k, 0, \dots, 0) \in R^{m \times n},$$

Here Σ_k is the same as Σ except that the smallest $n - k$ singular values are replaced by zeros. When the truncation parameter k is chosen properly, the condition number σ_1 / σ_k of the TSVD will be small, and so the problem is well conditioned. The TSVD solution then, $x_k = A_k^{-1} b$, where A_k^{-1} , is the pseudoinverse of matrix A_k is insensitive to noise in b and A . One observation is that TSVN regularization filters out the contributions to the solution corresponding to the smallest singular values.

2.2.4 Discrete Picard Condition

Equation 2.12 shows that for the solution x to converge, the SVD coefficients $|u_i^T b|$ must decay on average faster than the corresponding singular values σ_i . This condition is called the Discrete Picard Condition. If the Picard condition is satisfied, the regularized solution has same properties as exact solution, since the SVD components of the exact solution with largest magnitude are those coefficient that are well approximated, $u_i^T b / \sigma_i \approx u_i^T b^{exact} / \sigma_i$, (Hansen, 2001). Because of the presence of the noise, we don't expect to compute exact solution to the discrete inverse problem. Therefore, investigating Picard condition is necessary to find out whether a useful solution can be obtained. If the

Picard Condition is not satisfied, there is no reason to solve the ill-posed problem. To do this, we made the plots of the discrete Picard for the simulated EEG potential concerning all the three locations of the current dipoles (Superficial, at the middle and deeply located dipoles).

2.2.5 SVD and Tikonov Regularization

In case of Tikonov regularization, if we use the SVD decomposition of the matrix K in the solution (3), we get,

$$\begin{aligned}
J &= (K^T K + \alpha I)^{-1} K^T \Phi_{EEG} \\
&= (V \Sigma^T U^T U \Sigma V^T + \alpha V I V^T)^{-1} V \Sigma^T U^T \Phi_{EEG} \\
&= (V \Sigma^T \Sigma V^T + \alpha V I V^T)^{-1} V \Sigma^T U^T \Phi_{EEG} \\
&= V (\Sigma^T \Sigma + \alpha I)^{-1} \Sigma^T U^T \Phi_{EEG} \\
&= V \text{diag}((\sigma_i^2 + \alpha))^{-1} \Sigma^T U^T \Phi_{EEG} \\
&= V \text{diag}\left(\frac{\sigma_i^2}{\sigma_i^2 + \alpha} \times \frac{1}{\sigma_i}\right) U^T \Phi_{EEG} \\
&= \sum_i \left(\frac{\sigma_i^2}{\sigma_i^2 + \alpha}\right) \frac{u_i^T \Phi_{EEG}}{\sigma_i} \\
&= \sum_i f_i^\alpha \frac{u_i^T \Phi_{EEG}}{\sigma_i}
\end{aligned}$$

Comparing this regularized solution with the un-regularized solution (see Equation (2.12)), we see that the regularization adds a small value, $f_i^\alpha = \frac{\sigma_i^2}{\sigma_i^2 + \alpha}$, to the singular values. As α increases the solution becomes more stable. Further, we see that the filter factor f_i^α is close to one when σ_i is larger than α , corresponding to large contribution of the SVD

components to the solution. On the other hand, the SVD components are filtered out for σ_i much smaller than α ,

$$f_i^\alpha = \frac{\sigma_i^2}{\sigma_i^2 + \alpha} \approx \begin{cases} 1, & \sigma_i \gg \alpha \\ \frac{\sigma_i^2}{\alpha^2}, & \sigma_i \ll \alpha \end{cases}$$

2.3 Methods of Choosing Regularization Parameter

In this thesis, the methods we use to estimate the regularization parameter are, L-curve method, generalized cross validation (GCV) and normalized cumulative peirdogram (NCP). We present a theoretical illustration of these three methods.

2.3.1 L-Curve Method

The L-curve method (Hansen *et al*, 1993 and Hansen, 1994) considers a log-log plot of the regularized norm of the inverse solution versus the residual norm. The curve shows a trade-off between the size of the regularized term $||\Gamma J||^2$ and the data fitting term $||\Phi_{EEG} - KJ||^2$. The resulting shape has the shape of an 'L'. The optimal value of α corresponds to the corner of the curve since this point corresponds to a compromise between the two quantities. However, in practical applications the corner serves as a guide only since it is rarely provide the optimal solution. The corner of the curve can be computed by finding the maximum curvature of the curve κ (Hansen, 2001).

To find the curvature of the curve where the optimal value is assumed, we employ the Singular Value Decomposition (SVD) of the LFM matrix K

The SVD of matrix K is given by,

$$K = \sum_{i=1}^{3N} u_i \sigma_i v_i^T \quad (2.14)$$

where u_i and v_i are orthonormal singular vectors, σ_i is the singular values which appear in non-decreasing order. In terms of SVD of the LFM K , the regularized solution can be written as

$$J = \sum_{i=1}^{3N} f_i \frac{u_i^T \Phi_{EEG}}{\sigma_i} v_i \quad (2.15)$$

where $f_i = \frac{\sigma_i^2}{\sigma_i^2 + \alpha^2}$ is the Tikhonov filter.

Now, we can write the regularized and residual norms in terms of SVD,

$$\|J\|^2 = \sum_{i=1}^{3N} (f_i \frac{u_i^T \Phi_{EEG}}{\sigma_i} v_i)^2, \quad (2.16)$$

$$\|KJ - \Phi_{EEG}\|^2 = \sum_{i=1}^{3N} ((1 - f_i) u_i^T \Phi_{EEG})^2, \quad (2.17)$$

$$\eta = \|J\|^2, \rho = \|KJ - \Phi_{EEG}\|^2, \quad (2.18)$$

$$\hat{\eta} = \log \eta, \quad \hat{\rho} = \log \rho, \quad (2.19)$$

By plugging in the above expressions into the definition of the curvature from calculus, κ is given by (Hansen, 2001),

$$\kappa = 2 \frac{\hat{\eta} \hat{\rho} - \hat{\rho} \hat{\eta}}{((\hat{\rho})^2 + (\hat{\eta})^2)^{3/2}} \quad (2.20)$$

The corner of the curve separates the flat and vertical parts of the curve where the solution is dominated by regularization errors and perturbation errors, respectively. There are two limitations of the L-curve method (Hansen, 2001 and Hansen1994). The first one, is the faller of the method when the solution is very smooth, in which the SVD coefficients decay rapidly to zero, these solutions is dominated by the first few SVD components. The second one is related to the method asymptotic behavior. As the problem size increases, the method leads to over determined value of α . Both limitations depend on the characteristics of the particular problem being considered.

2.3.2 Generalized Cross Validation

This method (Golub *et al*, 1979 and Wahba, 1977) represents a statistical approach to choose the regularization parameter α . This technique has the following basic idea: the good value of regularization parameter should make $K J_\alpha$ able to predict the missing value in the right hand side (Φ_{exact} in our case). Therefore, the goal is to minimize the predictive mean-square error $\|KJ - \Phi_{exact}\|^2$. Because of Φ_{exact} is unknown, the GCV works instead with GCV function. So, the optimal value of α corresponds to the minimum value of the GCV function G ,

$$G_\alpha = \frac{\|KJ - \Phi_{EEG}\|^2}{(M - \sum_{i=1}^3 N f_i)^2} \quad (2.21)$$

Two difficulties of finding α using this method, the first one is due to the flat part, since GCV function has a very flat minimum, and it is not easy to

localize the minimum itself. The second difficulty is that GCV can sometimes mistaken correlated noise of a signal (Golub *et al*, 1979).

2.3.3 Normalized Cumulative Peirodogram (NCP)

In this technique, the strategy is to extract more statistical information about the Tikhonov residual vector r_α , by showing the relationship between the residual components and the amount of information that is available in the noisy data. The idea is to choose the largest regularization parameter that makes the residual vector resemble white noise vector (Wegman and Martinez, 2000; Hansen *et al*, 2006). We start to choose a large α and reduce it until having a residual vector that looks like white noise vector in terms of the frequencies of the power spectrum of the residual vector. Since the low frequency components of the exact solution Φ_{exact} will dominate its power spectrum, in contrast with power spectrum of the white noise components that will have the same expected value at all frequencies. This difference can be used to extract an optimal or near optimal regularization parameter.

According to singular value decomposition, we can express the residual vector in terms of singular vectors of Lead-field matrix K . The residual vector of the Tikhonov solution can be written as, $r_\alpha = \Phi_{EEG} - KJ = \sum_{i=k_c+1}^{3N} u_i^T f_i u_i \Phi_{EEG}$. Where k_c is the cut off index that separates the smallest singular values generated by noise in Φ_{EEG} from the largest singular values, and f is a high pass filter and equal to $\frac{\sigma_i^2}{\sigma_i^2 + \alpha^2}$. σ is the singular values of the matrix K . The optimum α is near the cut off index k_c .

NCP analysis considers the Φ_{exact} as a signal which appear distinctly different from the noise vector ϵ . The goal is to find alpha for which the residual changes behavior from being signal-like to being noise-like (Hansen *et al*, 2006).

This method views the residual vector as a time series (Hansen and Kilmer, 2007). It uses Fourier Transform to change the time domain of the residual vector to be in frequency domain in order to compute its normalized cumulative periodgram $C(r_\alpha)$. The power spectrum (peridogram) P_α of the residual vector r_α can be obtained by using Discrete Fourier transforms as

$$P_\alpha = (|\widehat{r}_1|^2, |\widehat{r}_2|^2, \dots, |\widehat{r}_{q+1}|^2)^T \quad (2.22)$$

The definition of the NCP for the Tikhonov residual vector r_α can be as the vector $C(r_\alpha)$ whose elements involve the cumulated sums of the power spectrum (Hansen *et al*, 2006),

$$C(r_\alpha)_i = \frac{(P_\alpha)_2 + \dots + (P_\alpha)_{i+1}}{(P_\alpha)_2 + \dots + (P_\alpha)_{q+1}} \quad (2.23)$$

The optimum alpha for NCP is the corresponding to the minimum value of the function D ,

$$D(\alpha) = \|C(r_\alpha) - C_{white}\|_2 \quad (2.24)$$

The advantage of this technique, its suitability for large scale problems, since it is computationally inexpensive (Hansen *et al*, 2006). However, the assumption of using standard parameter-choice methods, like the NCP

method, is that the right hand side Φ_{eeg} must satisfy the discrete Picard condition and it must consist of white noise.

2.4 Algorithms of solving the EEG Inverse Problem

In the literature, different localization methods with different techniques and algorithms have been developed to provide a solution to instantaneous, distributed, discrete, linear EEG inverse problem. In this subsection, we show three methods with brief mathematical details, which are Minimum Norm estimate MNE, weighted MNE, sLORETA and eLORETA.

2.4.1 Minimum Norm Estimate (MNE), $\Gamma = I$

The simplest constraint to apply is, $\Gamma = I$, which corresponding to Tikhonov regularization, and is the approach used in the Minimum Norm Estimate method (Hamalainen, 1984). This constraint corresponds to selecting the solution that has a minimum norm among the infinitely many possible solutions. In this case, the solution in Equation (2) becomes,

$$J = (K^T K + \alpha I)^{-1} K^T \Phi_{EEG} \quad (2.25)$$

The main concern about this approach is that there is no justification why the solution with the minimum norm is the best among all other solutions. Further, since the method selects the solution with minimum norm, this method is biased toward superficial sources (Pascual-Marqui, 1999), because less activity is required in superficial solution locations to give a certain surface potential distribution compared to deeper sources.

Consequently, MNE fails to address the issue of the deep sources onto the outermost cortex.

2.4.2 Weighted Minimum Norm Estimate (WMNE)

In order to handle deep current sources, different weighted strategies will be proposed. The weighted matrix is a structured block-diagonal matrix W , where all matrix elements are zero except for the diagonal sub-blocks denoted as $W_i \in \mathbb{R}^{3 \times 3}$. In this approach, each dipole has the same chance to be activated, even in deeper current sources.

The diagonally weighted MNE solution is given by,

$$\begin{aligned} J_w &= \arg \min ||\Phi_{EEG} - KJ||^2 + \alpha ||WJ||^2, \\ &= W^{-1}K^T [KW^{-1}K^T + \alpha I]^\dagger \Phi_{EEG} \end{aligned} \quad (2.26)$$

The following iterative algorithm converges to the block-diagonal weights W , (Pascual-Marqui et al, 2007),

1- Given the lead field matrix K , and a regularization parameter $\alpha \geq 0$

Initialize the weight matrix W as the identity matrix

2- Set $M = (KW^{-1}K^T + \alpha H)^\dagger$

3- For $j = 1 \dots N_v$ do:

The symmetric square root of the matrix $[K_i^T M K_i]$

4- Go to step 2 until no changes in W .

(where $H = I - 11^T/1^T 1$ with $H \in \mathbb{R}^{M \times M}$ denoting the centering matrix)

2.4.3 Standardized low resolution brain electromagnetic tomography (sLORETA)

The problem of addressing deep sources can be solved using sLORETA technique (Pascual-Marqui, 2002). sLORETA computes the statistical maps from the EEG/MEG data to localize the positions of the dipoles by standardizing the MNE current density using its variance. Statistical parametric maps combines the statistical interference which is based on standardized current density. This method gives zero localization error in absence of the noise. It takes into account the variance of both actual sources and noisy measurements (Pascual-Marqui, 2002). So, the electric potential variance is due to the noisy measurements $S_{\phi}^{noise} = \alpha H$ and actual (prior) source variance $S_J^{prior} = I, I \in \mathbb{R}^{3N \times 3N}$

$$S_{\phi} = K S_{J,prior} K^T + S_{\phi}^{noise} = K K^T + \alpha H \quad (2.27)$$

Where $H = I - 1 1^T / 1^T 1$ with $H \in \mathbb{R}^{M \times M}$ denoting the centering matrix which is the average reference operator (Pascual-Marqui, 2002).

The variance S_J of the estimated current density J is given by,

$$S_J = R = K^T [K S_{J,prior} K^T + \alpha I]^{\dagger} K \quad (2.28)$$

Where R is the resolution matrix. It can be seen as a linear projection from the original source dipoles to the variance estimation in absence of noise. Finally, sLORATA metric for the source location l corresponds to the

following estimates of standardized current density power (Pascual-Marqui, 2002).

$$\hat{j}_l^T [S_j]_{ll}^{-1} \hat{j}_l \quad (2.29)$$

Where $\hat{j}_l \in \mathbb{R}^{3 \times 1}$ is the current nsity estimate at the l^{th} voxel, and $[S_j]_{ll}$ is 3×3 block diagonal element.

2.4.4 Exact low resolution brain electromagnetic tomography (eLORETA)

There have been considerable efforts in order to reduce the localization error of the source localization by considering the weight matrix in a more appropriate way. eLORETA is a method gives solution with zero localization error even in the presence of the measurement and structural biological noise (Pascual-Marqui, 2007). This method was developed as working project in the University of Zurich in 2005(Pascual-Marqui, 2007).

Linear imaging methods are parameterized by a symmetric matrix $C \in \mathbb{R}^{N \times N}$, such that,

$$\hat{j}_i = [(K_i^T C K_i)^{-1/2} K_i^T C] \Phi \quad (2.30)$$

where $\hat{j}_i \in \mathbb{R}^{3 \times 1}$ is an estimator calculation for the electric neural activity at the i^{th} voxel, which could be current density.

In neuroimaging, localization inference based on the squared amplitude of the estimator for neuronal activity. The localization properties of a linear

imaging method are elaborated by considering the actual source as an arbitrary point in the j^{th} voxel, which assumes that,

$$\Phi = K_j A \quad (2.31)$$

where $K_j \in \mathbb{R}^{N \times 3}$ is a vector contains the potentials due to a certain source dipole with three coordinates, $A \in \mathbb{R}^{3 \times 1}$ and is an arbitrary vector contains non zero dipole moments for the source. By plugging equation (2.30) into equation (2.31) and taking the square amplitude, one can write for the estimation values as:

$$\|\hat{j}_i\|^2 = A^T K_j^T C K_i (K_i^T C K_i)^\dagger K_i^T C K_j A \quad (2.32)$$

For the case of eLORETA, the current density estimator at the i th voxel can be written as:

$$\hat{j}_i = W_i^{-1} K_i^T (K W^{-1} K^T + \alpha H)^\dagger \Phi \quad (2.33)$$

Where $W \in \mathbb{R}^{M \times M}$ is the symmetric weight matrix, where all its elements are zero except for the diagonal sub-blocks. The exact zero localization can be achieved when weights W_i satisfy the equation,

$$W_i = [K_i^T (K W^{-1} K^T + \alpha H)^\dagger K_i]^{1/2} \quad (2.34)$$

2.5 Localization Error Evaluation Measures

In this study, we considered three error measures to evaluate the influence of the number of scalp sensors N_e and solution space resolution on the source localization accuracy. The first measure is the Localization error (Pascual- Marqui, 2002). It was defined as the distance between the actual test source and the location of the maximum estimated current.

The second measure is the spatial spreading or blurring of the solution (Pascual-Marqui, 1999). It corresponds to a measure of spatial standard deviation of the imaging method centered at the actual test sources. Defined as,

$$Spreading = \sqrt{\frac{\sum_{i=1}^M \|r_i - r_{test}\|^2 \|\hat{j}_i\|^2}{\sum_{i=1}^M \|\hat{j}_i\|^2}} \quad (2.35)$$

where r_{test} is the actual test dipole location, r_i is the location of the i^{th} source, and \hat{j}_i is the estimate of the current density.

The final measure that we used is the Eculidean distance between the actual dipole location and the center of gravity (COG) of eLORETA source estimate scores, defined as (Salman *et al*, 2014), (Baillet, 1998),

$$COG = \left| \frac{\sum_{i=1}^M \|\hat{j}_i\| \|\hat{r}_i\|}{\sum_{i=1}^M \|\hat{j}_i\|} \|\hat{r}_{test}\| \right| \quad (2.36)$$

Chapter Three

Methodology

3.1 Introduction

Solving the source localization problem using the distributed dipole model approach require first solving the forward problem that maps a current source generator inside the brain to the scalp potentials at the electrodes. The forward problem is a well posed problem that have a unique solution. We used an efficient FDM solver that we already have (Salman *et al*, 2014) to obtain the forward solution. Then, the forward solver is used to generate a generic LFM (gLFM) that maps the current source generators modeled as current dipoles placed at every gray matter voxel in the brain to the scalp potentials at the electrodes. Once, the gLFM is obtained for a head model, a LFM can be obtained by down sampling from the generic LFM as discussed below.

After calculating the LFM, we tested whether a useful solution of the ill-posed problem is possible or not using the Picard Condition test. Then, a simulated EEG data corresponding to different current dipole sources, placed at known locations, are generated. For each location, we considered several dipole orientations. Then, for each simulated EEG data set, several white Gaussian noise level was considered in the evaluation.

In this study we considered two distributed dipole methods, the MNE and the eLORETA. For each method, we used three automatic regularization parameters methods, L-curve, GCV, and NCB. Then we compared the solution obtained in each case for each simulated EEG data with the exact known solution using three measures described in section (2.5). The gLFM was generated in previous work using high performance computing solver implemented in c++. The rest of the work was done using Matlab.

In this chapter we describe the methodology we used in conducting the study. The chapter is organized as follows. In section 3.2 and 3.3, the computational head model and the generation of the gLFM are discussed, respectively. In section 3.4, down sampling a LFM from the gLFM is described. In section 3.5, we provide detailed discussion about the generation of the simulated EEG data with different noise level. In Section 3.6, we present the methodology in obtaining the regularization parameter α and solving the Inverse Problem.

3.2 Modeling the Human Head Electromagnetic

To solve the forward problem described in Section (2.1), first we need to build a computational head model. In this model, the human head is modeled as a volume conductor consists of 5 different uniform tissues. The computational model requires a geometry model of the different tissues of human head, and a conductivity model to assign a conductivity for each tissue.

The geometry model, the geometry model defines the boundaries between different tissues of the human head. Medical imaging such as Magnetic Resonance Imaging (MRI) provide images of anatomical details with resolution better than 1mm^3 . These images can be segmented to a number of tissues where each tissue is assumed to have uniform electrical properties. In this study, we used the geometrical model obtained from an MRI image with resolution of 1mm^3 for a subject, segmented into five uniform tissues, white matter, gray matter, CSF, skull and scalp. Figure (3.1) shows these tissues. The segmented image is obtained from previous work done at Neuroinformatic Center (University of Oregon) and Electrical Geodesics Incorporated (EGI).

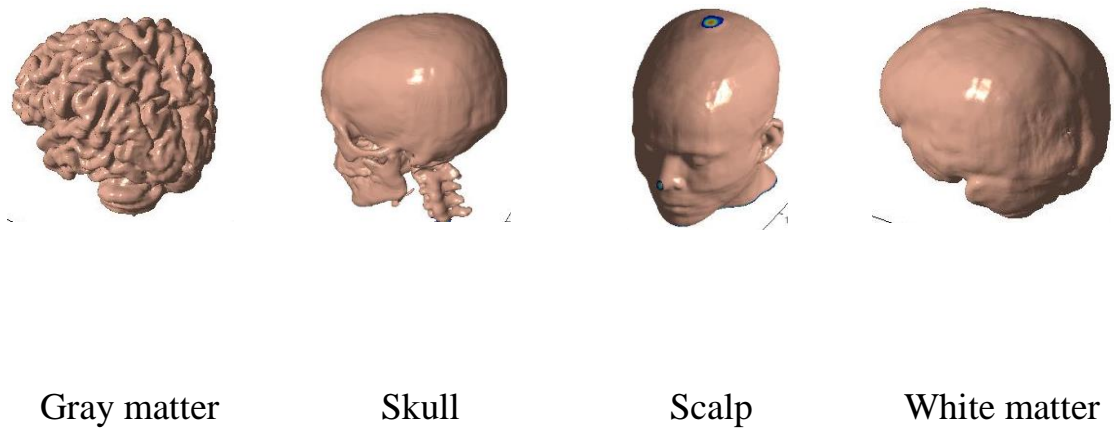


Fig. (3.1): Geometric model of the tissues of the human head

The conductivity model, once different tissues of the human head are identified from the segmented MRI image, a conductivity model and values must be specified. In this study we assumed the conductivities of

all tissues are isotropic and have values obtained from the literature and shown in Table (3.1).

Table (3.1): Tissues Parameters in realistic head model (Salman *et al*, Ferree *et al*, 2000)

Tissue Type	$\sigma(\Omega^{-1}m^{-1})$	Reference
Gray matter	0.25	Geddes (1967)
Csf	1.79	Daumann (1997)
Skull	0.0180	Law (1993)
Scalp	0.44	Burger (1943)
White matter	0.35	Ferree (2000)

The forward solver algorithm, In this study we used the Alternating Direction Implicit (ADI) method, which is a finite difference method FDM to solve Poisson equation as described in Section (2.1). The solver was implemented in previous work (Salman *et al*, 2014). The solver is efficient and can handle only isotropic tissues. Using the forward solver, we can calculate the potential at the scalp electrodes for a given current source modeled as a current dipole inside the brain.

The current source model, it is well accepted to model a current source generator inside the brain as a current dipole consists of a current source and a current sink placed close to each other. To obtain the potential due to a current dipole source with arbitrary orientation, we first computed the potential due to three orthogonal unit dipoles placed along the x-, y-, and z-axis to obtain their potentials φ_x , φ_y , and φ_z , respectively, at the scalp electrodes. Then, since Poisson equation is linear regarding current sources, the potential corresponding to a dipole placed at the three

orthogonal dipoles location with arbitrary orientation, given by the direction cosines (α, β, γ) can be calculated by the superposition principle,

$$\varphi = \alpha\varphi_x + \beta\varphi_y + \gamma\varphi_z \quad (3.1)$$

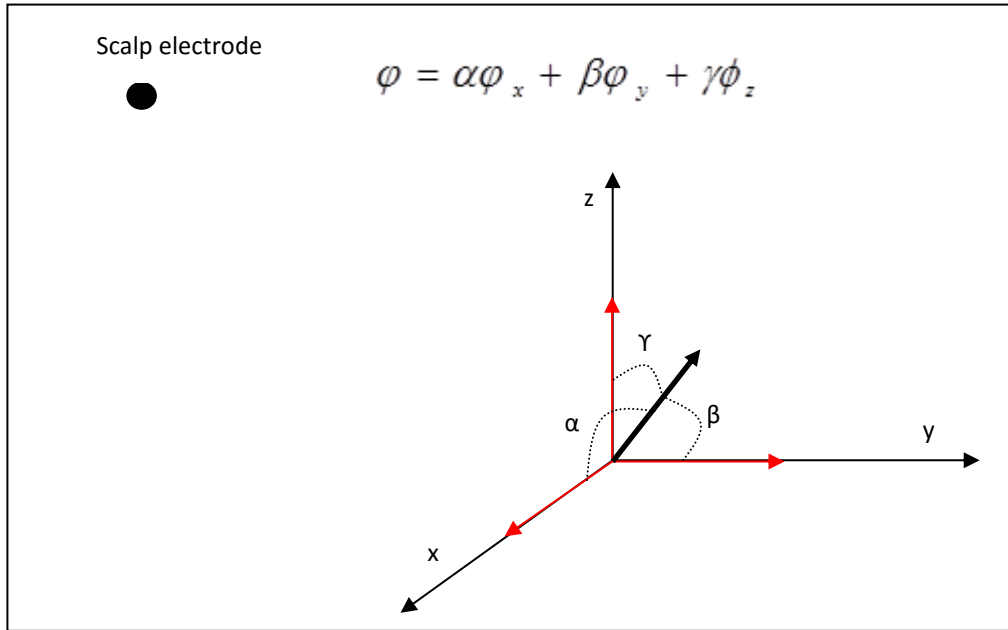


Fig.(3.2): The potential corresponding to a dipole with arbitrary orientation is a linear combination of the potential due to three orthogonal unit dipoles.

3.3 The generics LFM (gLFM)

The generic Lead Field Matrix (gLFM) construct introduced in (Salman *et al*, 2014) serves as generators of LFMs. It maps the orthogonal generic dipolar sources to generic electrodes potentials. Three orthogonal generic distributed dipoles are placed at every voxel in the gray matter and the generic electrodes are placed at 1mm^3 inter-spacings on the scalp. Once a gLFM is computed using the forward solver, many different LFMs can

be sampled based on different constraints or resolution imposed on the sources (e.g., the number and locations of the electrodes). This can be achieved efficiently by sampling from the rows and columns of the gLFM appropriately. The computation of a gLFM factor out the common and computationally intensive part of the analysis from the application of different inverse algorithms. In the case of distributed dipole models, the appropriate columns corresponding to imposing constraints on the sources are sampled as well. Then different distributed dipoles algorithms can be applied. In this study we used a gLFM matrix that was computed previously at University of Oregon computing cluster. The structure of the gLFM is shown below,

$$\begin{bmatrix} \phi_{11}^x & \phi_{11}^y & \phi_{11}^z & \cdots & \phi_{1N}^x & \phi_{1N}^y & \phi_{1N}^z \\ \vdots & \vdots & \vdots & \vdots & \vdots & \vdots & \vdots \\ \phi_{M1}^x & \phi_{M1}^x & \phi_{M1}^x & & \phi_{MN}^x & \phi_{MN}^x & \phi_{MN}^x \end{bmatrix}$$

where, each row contains the potential due to three orthogonal dipole moments placed at every dipole location at a scalp electrode. And, every three column correspond to the potential due to three orthogonal dipoles at all electrodes.

3.4 Sampling the Lead field Matrix

Different LFMs with different distributed dipoles configuration and different scalp electrodes configuration can be down sampled from the gLFM. This is achieved by down sampling from the rows and columns

of the gLFM. In this study, we selected 128-electrodes uniformly distributed on the scalp from the generic electrodes and we sampled 2500 current dipoles from the generic distributed dipoles, using the method illustrated in (Salman *et al*, 2014) at resolution of 7 mm. Fig.(2), shows a distributed dipoles sampling at resolution of 7 mm.

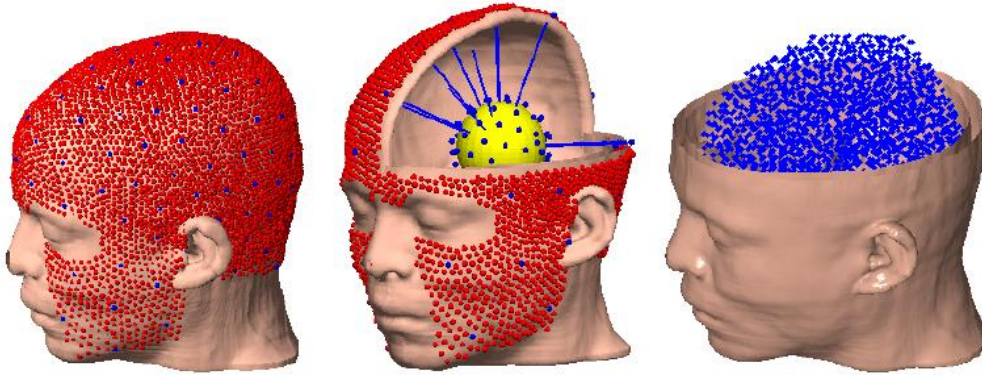


Fig.(3.3): Generic scalp sensors (red) and 128-sampled scalp sensors (blue) (left). Sampling 64-sensors using uniformly distributed points on a unit sphere (middle). Sampling distributed dipoles at resolution of 7 mm (right) (Salman *et al*, 2014).

3.5 EEG Simulated data (Synthetic Data)

To test the accuracy of the inverse solution using different automatic regularization parameter tuning methods, we simulated the EEG data corresponding to a current dipole source placed at certain location and have a certain orientation as follows,

- 1) From the generic dipoles set, we selected a dipole in a location p .
- 2) The potentials $\varphi_x, \varphi_y, \varphi_z$ due to the three orthogonal dipoles d_x, d_y, d_z

in that location at the electrodes are then extracted from the gLFM.

- 3) For a certain dipole moment orientation (α, β, γ) , we calculated the potential using Equation 3.1, to obtain the simulated EEG potential, $\varphi_{EEG} = \alpha\varphi_x + \beta\varphi_y + \gamma\varphi_z$.
- 4) A white Gaussian noise with different levels is added to φ_{EEG} , to simulate noisy data. We used the Matlab function `awgn()` to generate the white Gaussian noise. This new generated potential vector represents the EEG potentials $\Phi_{EEG} \in \mathbb{R}^{M \times 1}$.

3.6 Tuning the regularization parameter α and solving the Inverse Problem

For this study, we selected several EEG data sets as described above corresponding to three locations inside the brain. One location is superficial (D1), which is close to the surface of the brain. The second location is in the middle region of the brain, at about the middle distance between the center of the brain and the surface of the brain (D2). The third location is deep inside the brain close to the center (D3). The reason for these choices is to include into consideration the fact that the MNE method is biased toward superficial sources. Table (2) shows the id's and the coordinates of the selected three dipole locations.

Table (3.2): The Identification number and the coordinates of each selected dipole at the solution space.

Location at the cortex	ID	Coordinates		
		X	Y	Z
Superficial	147633	82	101	212
At the middle	409823	161	84	146
Deep	215425	99	100	143

For each dipole location we considered 30 different orientations selected by uniformly distributing 30 points on a unit sphere centered at each dipole location as shown in Figure (3.3). For each dipole location and orientation we considered 128 electrodes uniformly distributed on the scalp. Then, we used distributed dipole grid spacing of 7 mm to localize each dipole location and orientation. We considered three measures to evaluate the source localization accuracy when applying the L-curve, GCV, and NCB methods for tuning the regularization parameter. The first measure is the Euclidean distance between the actual dipole location and the location of the dipole with maximum estimated current. The second measure is the Euclidean distance between the actual dipole location and the location of the center of gravity (COG) of the sources estimated current (localization error) computed by the inverse method. The third measure is the spatial spreading or blurring of the estimated currents as described in Section (2.6). For each location the average localization error of the 30 dipole orientations is evaluated and considered as the error. This evaluation is repeated twice, first by using the MNE inverse method and the second by using the WMNE method.

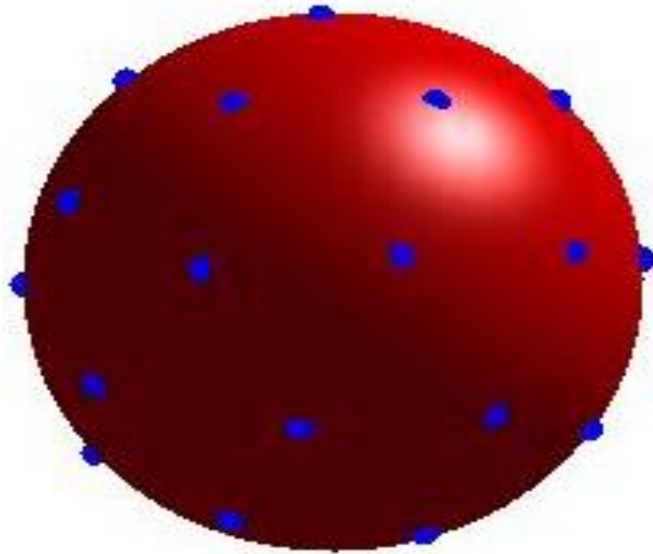


Fig.(3.3): 30 points uniformly distributed on a unit sphere, each point represents one orientation.

Chapter Four

Results and Calculations

4.1 Discrete Picard Plots

All data and figures were analyzed using Matlab software. As a first step in solving the EEG inverse problem, the Discrete Picard Plots were obtained for the simulated EEG data sets corresponding to the dipole locations D1, D2 and D3. The simulated EEG data is obtained for the radial orientations of these test dipoles. A noise level of SNR ratio of 4 and 12 is added to the simulated EEG data sets. Figure (4.1) shows the Discrete Picard Plots of these data sets. The Discrete Picard Plots describes the decaying rate of the absolute values of the SVD coefficients ($u_i^T \Phi_{EEG}$) and the decaying rate of the corresponding singular values σ_i in addition to the decaying rate of their ratio.

We found that, the Discrete Picard Condition is satisfied for all data sets. It is clear from the plots that the rate of decay of the Fourier coefficients (black stars) is fairly faster than the decay rate of the singular values (blue dots) for small indexed singular values, as shown in the figure. For higher singular values the decay rate of the singular values becomes faster. These singular values correspond to noise and must be truncated to obtain a useful solution as discussed in Section (2.2.3). Also, we see in the figure that the rate of the decay of the Fourier coefficients increases as the SNR increases for the small indexed singular values as expected. Further, we

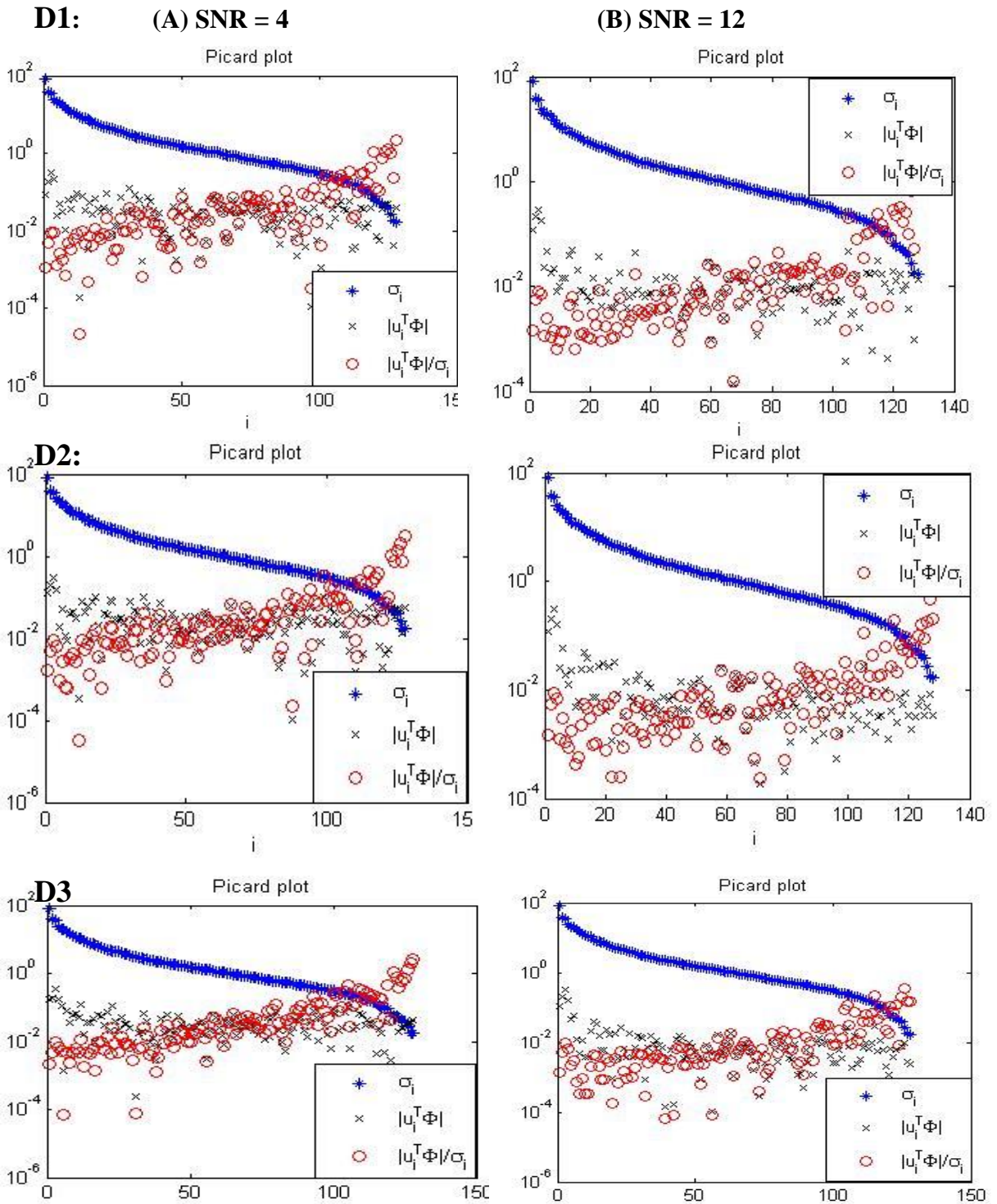


Fig. (4.1): Discrete Picard Plots for the D3 with radial orientation at different SNR (4, 8, 12 and 16). The blue dots are the singular values, the Fourier coefficients are shown in green and red circles are Fourier coefficients divided by singular values.

see that the location of the dipole does not affect the decaying rate of the singular values and the Fourier coefficients. However, we must consider more locations to make such a conclusion. The satisfaction of the Picard condition indicates that it is possible to obtain a useful solution for the ill-posed problem.

4.2 The L-curve, GCV and NCP curves

We computed the regularization parameter using the simulated EEG data sets corresponding to the three dipole locations with different orientations using L-curve, GCV and NCP methods. We added different levels of noise to the simulated EEG data. The results of these methods and their curves is discussed in the following subsections.

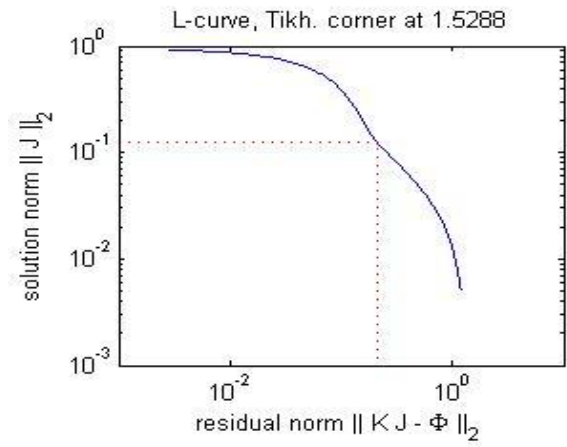
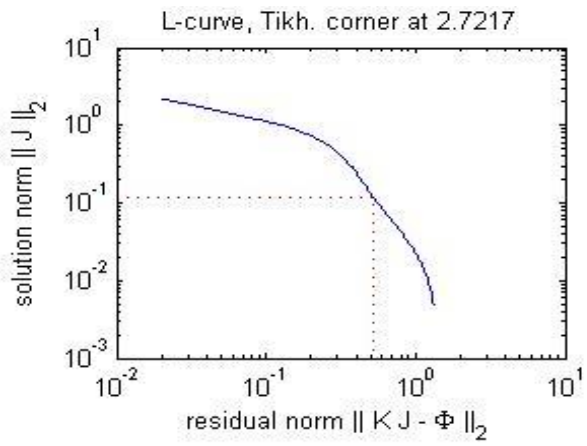
4.2.1 The L-curve

The L-curves corresponding to the three data sets are shown in Fig. (4.2). From these figures, we see that the shape of the L-curve converges to its characteristic shape 'L' and gives a clear corner for the three data sets. However, when we choose larger SNR, we see a better convergence and the corner of the curve manifested better. Further, we see that for data sets corresponding to the shallow dipole (D1), the curve converges better and the corner appears better compared to the data sets corresponding to deeper current dipoles.

D1:

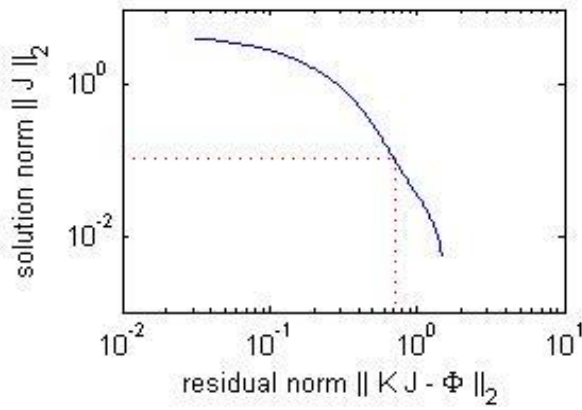
(A) SNR = 4

(B) SNR = 12

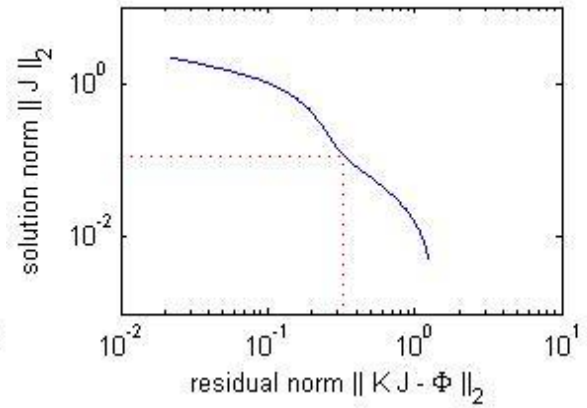


D 2:

L-curve, Tikh. corner at 3.8049

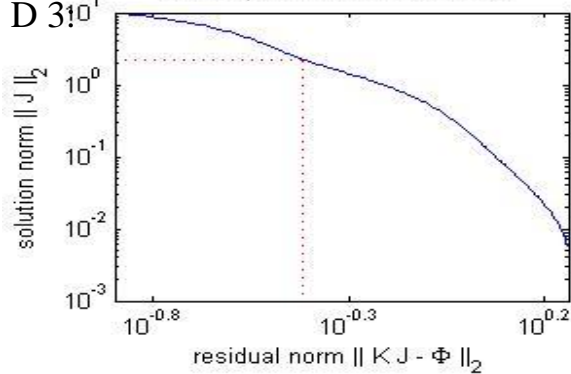


L-curve, Tikh. corner at 2.044



D 3:

L-curve, Tikh. corner at 0.12093



L-curve, Tikh. corner at 4.5434

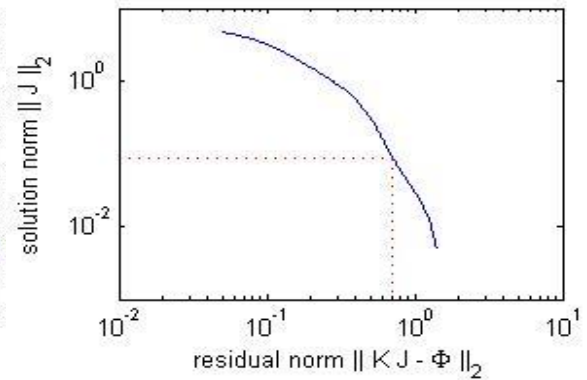


Fig. (4.2): The L-curve for D1, D2 and D3, for two signal to noise ratios (4 and 12). The residual norm is on x-axis and solution norm on the y-axis.

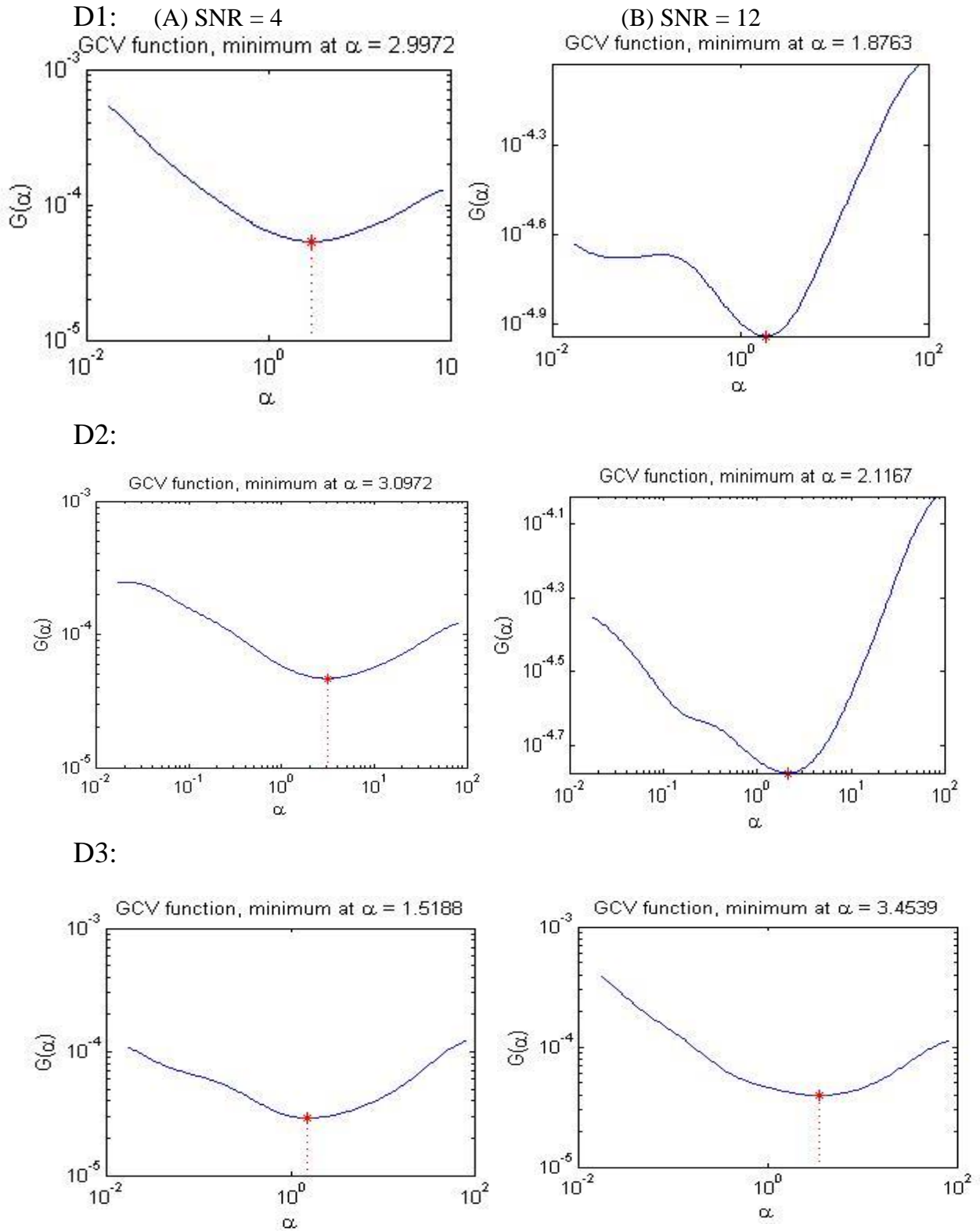


Fig. (4.3): The GCV functional for D1, D2 and D3 for two levels of SNR (4 and 12). The regularization parameter is on x-axis and GCV functional on the y-axis.

4.2.2 The GCV functional curve

Using the same three data sets that we used for the L-curve method, we plotted the GCV function curves discussed in Section (2.3.2) using two levels of added SNR noise of 4 and 12. We see from the plots shown in Fig. (4.3) that the GCV curves have a clear minimum for all data sets when both values of the SNR are used. However, for smaller SNR, the GCV curves look somewhat flat. It is slightly different from its characteristic shape.

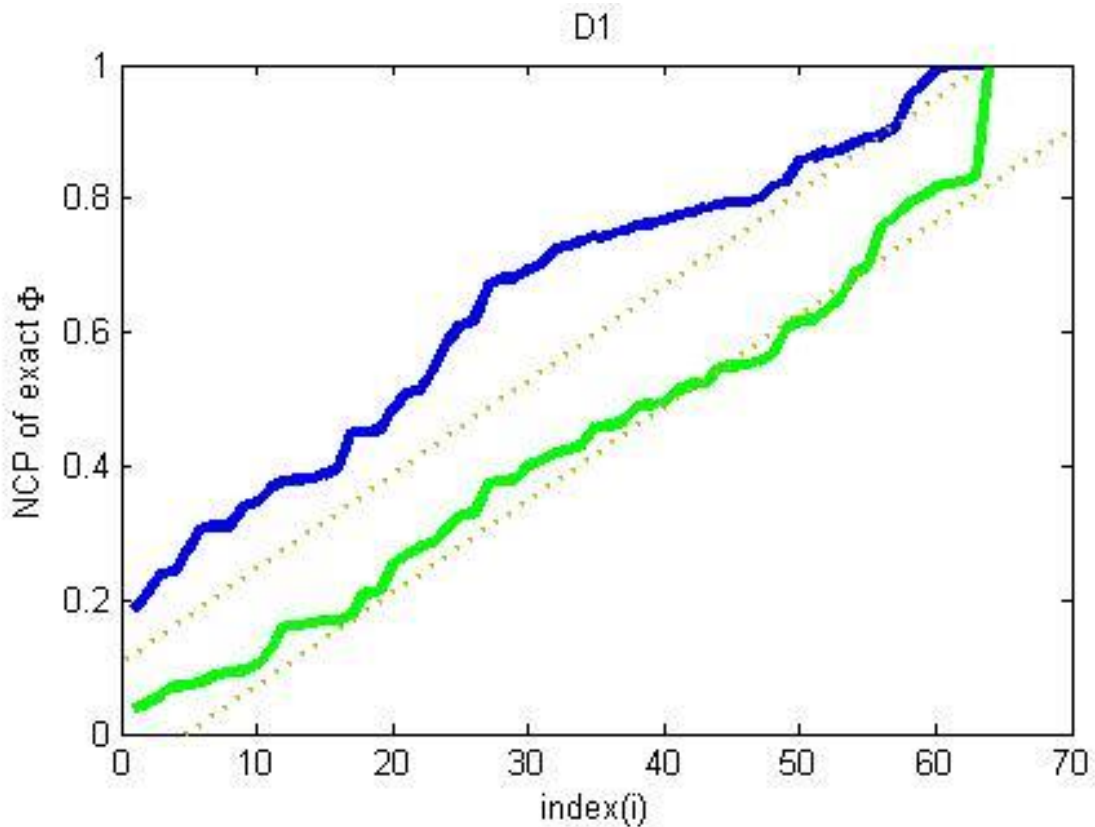


Fig.(4.4): The NCPs for the synthetic exact ϕ (Blue line), and the NCP of the synthetic data after adding white Gaussian noise.

4.2.3 NCP curves

❖ NCPs of the exact Φ

As a first step, in order to observe the effect of the white Gaussian noise, we plotted the NCP of the simulated EEG data Φ corresponding to the dipole location D1 without noise and after adding white noise with SNR = 6. In Fig.(4.4), we see that the noisy data set Φ (green line) fits within Kolmogorov-Smirnoff (KS) limits, which means that it is dominated by low frequency components. The two gray lines in the figure correspond to the KS limits.

❖ Estimation of α using NCP method, NCPs curves

The NCPs curves for the three simulated EEG data sets corresponding to the dipoles (D1, D2 and D3) with radial orientation are shown in Fig. (4.5). As the figure shows, some curves have a high frequency component, while others have a low frequency components. Curves above the blue line correspond to high frequency components. While those below the blue line corresponds to low frequency component. The blue line represents the optimal NCP, which corresponds to the optimal regularization parameter. On the other hand, for smaller SNR = 4, most of the NCP curves are below the blue line KS, corresponds to low frequency components. This means that these components have higher white noise compared to 16-SNR case as expected. Also, we can see that for deep current sources in the brain (D3 and D2), the NCPs of the residual vector become closer to each other and they fit within KS limits. The difference can be noticed in the Fig. (4.5) part A.

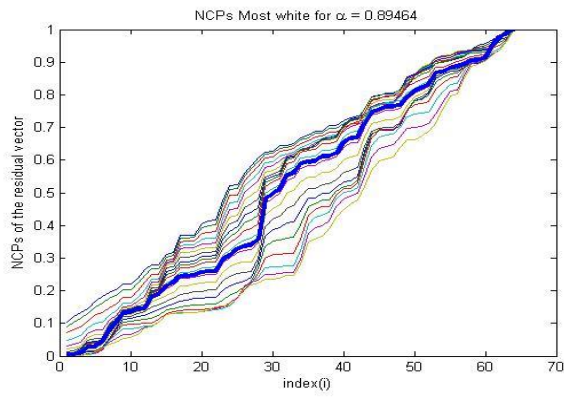
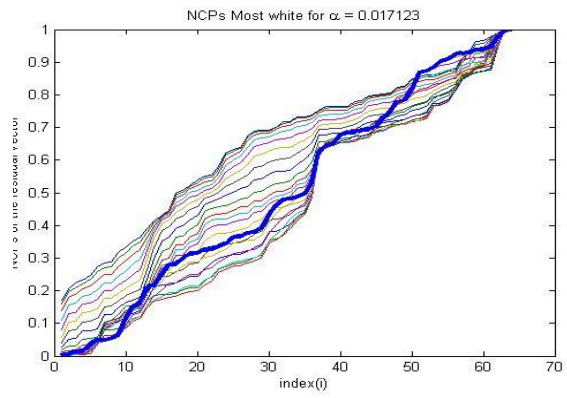
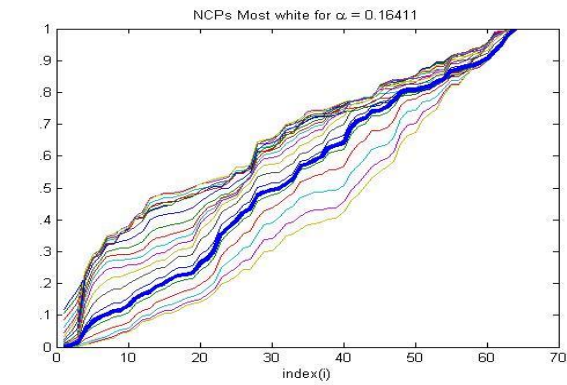
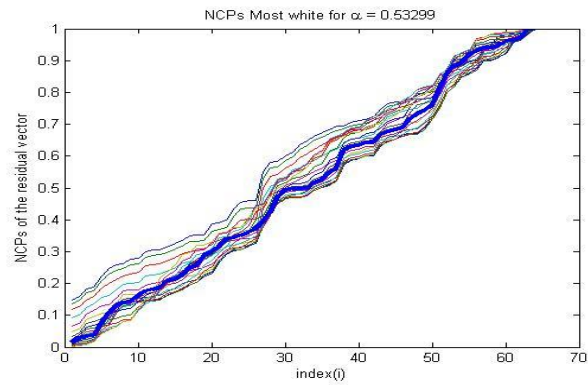
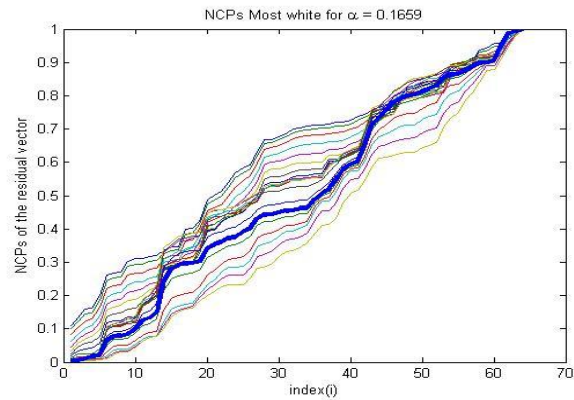
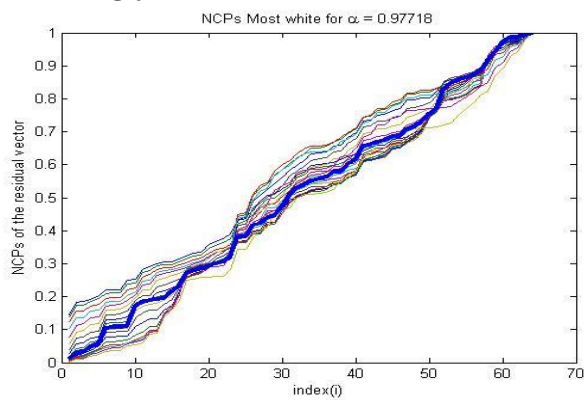
D1: (A) SNR = 4**(B) SNR = 12****D2:****D3:**

Fig. (4.5): The NCPs curves for shallow (D1), mid (D2), deep (D3) dipoles for two levels of signal to noise ratio (from left to right). The red thick line represents the optimum NCP, which corresponds to the optimum regularization parameter.

Table (4.1): A Comparison between the regularization parameters, obtained using L-curve, GCV and NCP methods using different SNR for simulated EEG data corresponds to three dipole locations and different radial orientations.

Location at the cortex	SNR	L-curve	GCV	NCP
Superficial (D1)	4	2.7217	2.9972	0.8946
Superficial (D1)	12	1.5288	1.8763	0.0172
At the middle (D2)	4	3.8049	3.0972	0.5322
At the middle (D2)	12	2.0440	2.1167	0.1641
Deep (D3)	4	0.1209	1.5188	0.9771
Deep (D3)	12	4.5434	3.4539	0.1659

Table (4.1) lists the values of the regularization parameter α obtained using the three methods and the three simulated data sets with different SNRs. It can be seen that each method generates different value of α . This simply reflects the fact that a unique solution of the ill posed problems does not exist. Our goal is to find an optimal one. In the next section, we show our results obtained by solving the EEG inverse problem and finding an estimate of the current sources J that explain the simulated EEG data. WMNE algorithm is used to solve the inverse problem.

4.3 Solving the Inverse Problem

In this section, we present the results of our comparative study between the accuracy of the solution of the EEG inverse problem obtained using two inverse algorithms, weighted minimum norm estimate (WMNE) and eLORETA. For each inverse method, we used the regularization parameter obtained using the L-curve, GCV and NCP methods.

First, we generated simulated EEG data sets using the procedure described in Section (3.5). These data sets correspond to three dipole locations listed in Table (3.2). For each dipole location, we considered 30 different radial orientations. These orientations are generated by uniformly distributing 30 points on a unit sphere centered at the dipole location. Next, the potential corresponds to each dipole location and orientation is sampled from the gLFM, and different noise levels are added. This procedure is described in details in Section (3.5). Next, for each simulated EEG data set, we found the regularization parameter using the three methods (L-curve, GCV and NCP). These values of the regularization parameters are then used in solving the inverse problem 30 times for each inverse method, WMNE and eLORETA. For each solution, we calculated the three measures described in Section (2.6), localization error, center of gravity and spatial spreading,. Finally, we computed the mean and the standard deviation of the 30 error measures. This procedure was repeated for each test dipole location D1, D2, and D3. The results were evaluated by plotting the means of measures as a function of noise level.

4.3.1 Estimating the solution using WMNE algorithm

Here we present the results obtained using WMNE algorithm. We solved the problem using the regularization parameter computed by the three methods (L-curve, GCV and NCP). Fig. (4.6), (4.7) and (4.8) shows the

Shallow dipole

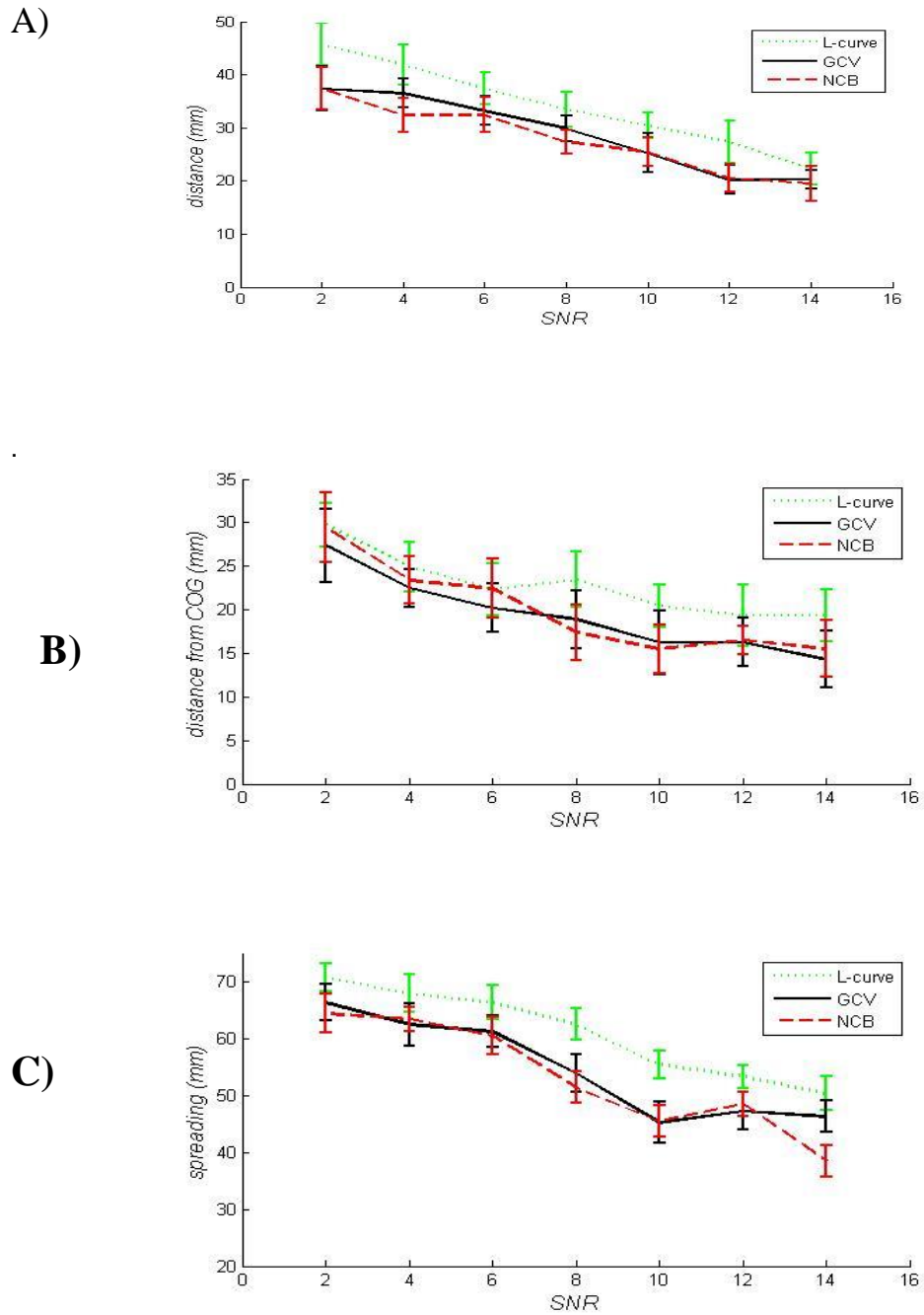


Fig.(4.6): Using WMNE algorithm, for shallow dipole , A) The localization error (mm) in terms of SNR after obtaining α from L-curve, GCV and NCP. B) Distance from the center of gravity (mm) in terms of SNR. C) Spatial spreading in terms of SNR.

Results in terms of the three error measures, localization error, center of gravity and spatial spreading, respectively.

Fig.(4.6.a), Fig.(4.7.a) and Fig.(4.8.a) show the localization measures obtained by using WMNE method. For these solutions the optimal regularization parameter α was obtained using the L-curve (green line), GCV (black line) and NCP (red line). The synthetic data sets used corresponds to three test dipole locations. The first data set corresponds to a shallow current dipole location close to the surface of the brain. The second (middle) corresponds to dipole location at the middle distance between the center of the brain and the surface. The third dipole (deep) corresponds to dipole locations close to the center of the brain.

It can be seen that for the three dipole locations, the localization error is highest when WMNE method uses the regularization parameter obtained using the L-curve method compared to those obtained when using the NCP and GCV method. On the other hand, the localization error is smaller when WMNE algorithm uses the NCP methods compared to the error obtained when GCV method is used. For instance at SNR = 14, the error was 22.3 mm when using the L-curve compared to 20.2 mm when using GCV and 19.4 mm when using NCP.

Furthermore, it is clear that the localization errors decrease with increasing the signal-to-noise ratio (SNR) when using the three methods for all dipole locations. These results agree with the intuition. Further, we see that the localization error is slightly increases at SNR values of 2 and 4 as

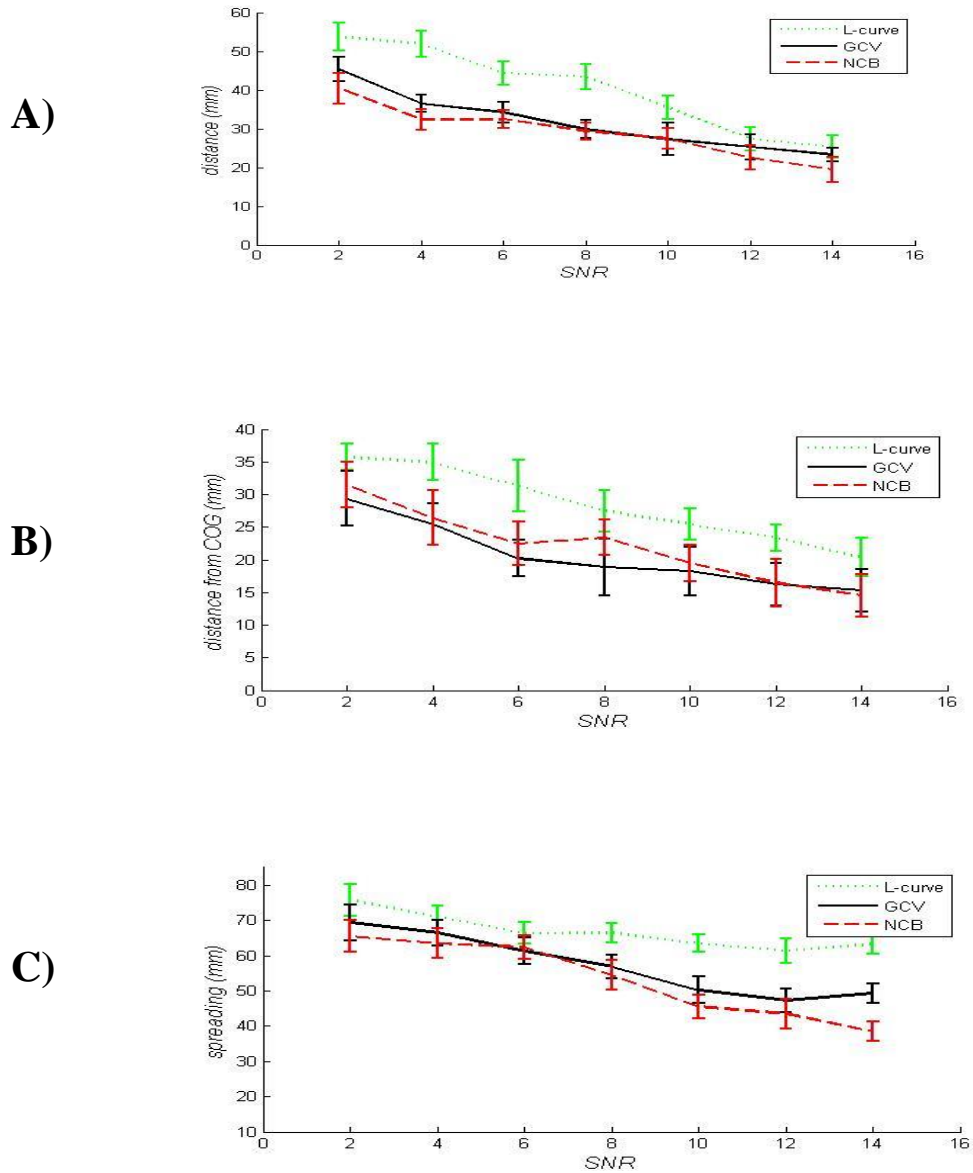
Mid dipole:

Fig. (4.7): Using WMNE algorithm, for mid located dipole, A) The localization error (mm) in terms of SNR after obtaining α from L-curve, GCV and NCP. B) Distance from the center of gravity (mm) in terms of SNR. C) Show the spatial spreading in terms of SNR.

Deep dipole:

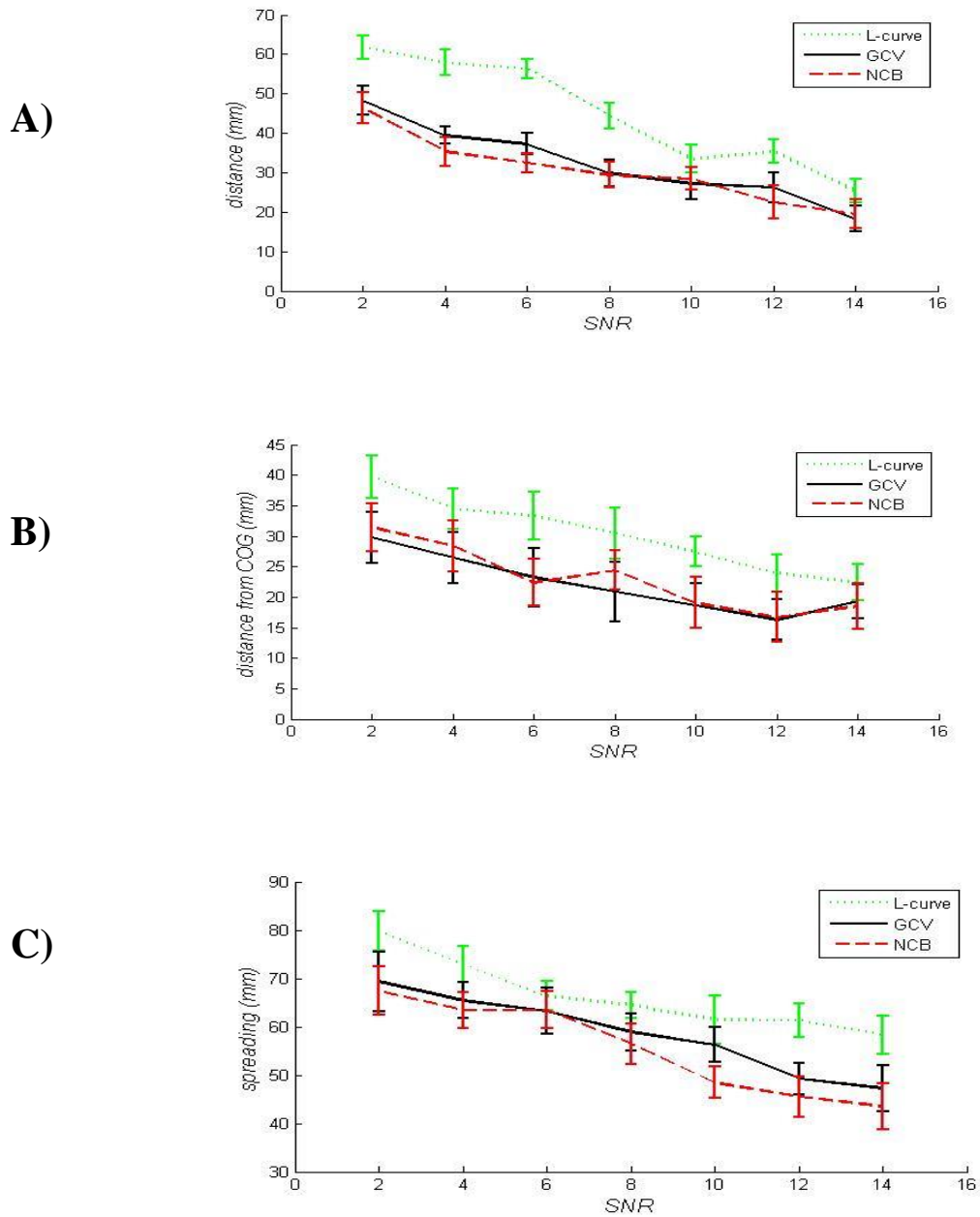


Fig. (4.8): Using WMNE algorithm, for deep located dipole, A) The localization error (mm) in terms of SNR after obtaining α from L-curve, GCV and NCB. B) Distance from the center of gravity (mm) in terms of SNR. C) Spatial spreading (mm) in terms of SNR.

the depth of the test dipole location increases, but it does not change much at $\text{SNR} = 14$. These results indicate that the WMNE can overcome the bias toward superficial sources of the MNE method and the method can handle deep current source generators as well. These error results are the average of using 30 uniformly distributed orientations for each test dipole location.

Fig. (4.6.b), Fig. (4.7.b) and Fig. (4.8.b) show the errors measure defined as the distance of the location of the center of gravity of the estimated current to the actual dipole location (COG error). Using this measure, our results indicate similar to localization error measure performance result. It can be seen that when α , obtained using the L-curve method, used in the WMNE, the COG error is the highest for the three dipole locations. In contrast, the accuracy obtained using the NCP and GCV methods are almost the same according to this measure. However, in some cases the GCV method outperforms the NCP method. Furthermore, it is clear that the COG measure decreases with increasing the signal to noise ratio when using the three methods for the all data sets corresponding to three dipole locations. According to this measure, a small increase in the errors is noticed when we move from the superficial dipole to deep dipole locations, in particular when we used low SNRs, such as 2 and 4, as it is shown in Fig. (4.6.b), Fig.(4.7.b) and Fig.(4.8.b). But, when $\text{SNR} = 12$, or 14, the positions of the dipole did not affect the COG error, since they reach the same amount of errors.

The third measure we considered is the spatial spreading, which provides a measure of how the solution is focused in space. A focused solution gives a distribution of the estimated current values such that it is high around the active region while it is low far away from the active region. It is desired to obtain a focused solution. According to the spatial spreading measure, our result shown in Fig.(4.6.c), Fig.(4.7.c) and Fig.(4.8.c), indicate that the solution obtained using the L-curve gives the least focused solution compared to the solution obtained using the NCP and GCV methods. Further, solutions obtained using the NCP are slightly more focused than the solution obtained using GCV method. Further, it is clear that the spatial spreading measure decrease with increasing the signal to noise ratio, which means larger noise produce blurred less focused solutions. Moreover, the focus of the solution remains the same as we move to deeper locations.

In summary, for the three measures, the algorithm gives the highest errors when it uses α obtained using L-curve, then GCV and NCP, respectively. Although, the algorithm with α obtained using GCV method sometimes gives error values similar to these obtained using the NCP method. Also, WMNE handled the three locations without any bias, since it gives similar localization error at the three dipole locations.

4.3.2 Solving the inverse problem using eLORETA and sLORETA

In this section, we solved the inverse problem using sLORETA and eLORETA algorithms. The regularization parameter inserted into the algorithms manually. The results are shown as a comparative study

between sLORETA and eLORETA. We choose the dipole to be in the middle to generate the simulated EEG data, the orientation of the dipole . After that, we calculated the errors using the previous illustrated measures.

Fig.(4.9.a), shows the localization error (in mm) for both eLORETA and sLORETA at different signal to noise ratios. It's clear that eLORETA gives small amount of errors in a comparison with sLORETA. Further, eLORETA reached zero localization error even in the presence of the noise at (SNR =10), while sLORETA did not.

Fig.(4.9.b), illustrates the center of gravity errors (in mm) for eLORETA and sLORETA at different signal to noise ratios. eLORETA also gives better results than sLORETA at all levels of signal to noise ratio. eLORETA reached the zero error even in the presence of the noise.

Fig.(4.9.c), shows the spatial spreading errors, for eLORETA and sLORETA at different signal to noise ratios. Its noticeable that eLORETA also gives better results than sLORETA at all levels of signal to noise ratio. Since when the SNR was to be equal 14, the error was to 25, whereas, sLORETA gives larger error (35).

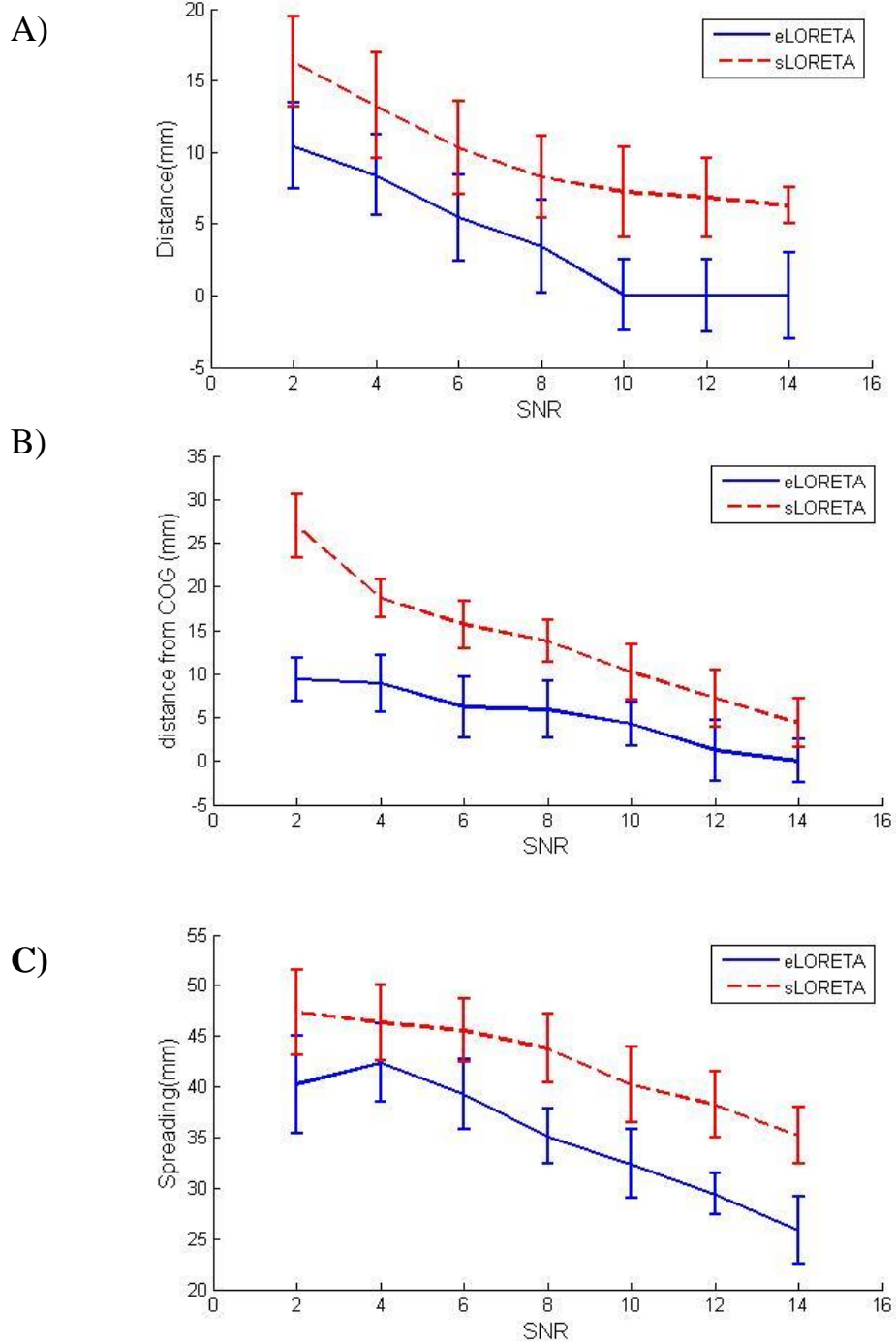


Fig.(4.9): Blue line (eLORETA), red line (sLORETA), A) Localization errors using eLORETA and sLORETA at different signal to noise ratio. B) Center of gravity errors, C) spatial spreading measure.

Chapter Five

Conclusion

In this thesis, we solved the inverse problem of the source localization of the EEG signals. Source localization aims to find the sources of the neural activities inside the brain. The inverse ill-posed problem is characterized with a difficulty of tuning the regularization parameter of the Tikhonov regularization. As a comparative study, we applied three automatic regularization parameter selection methods (L-curve, GCV and NCP) to find an optimal regularization parameter that improves the localization error in finding an estimated solution of the problem. WMNE algorithm is used as a solver of the inverse problem. In the first part of the thesis, we considered several radial orientations of the current dipole.

Three dipole locations have been selected to generate the synthetic EEG data (shallow location, at the middle of the cortex and deep located dipole) with different noise levels.

The application of the L-curve and NCP methods, requires the problem to satisfy the Picard Condition and the noise must be white Gaussian. In order to check the satisfaction of these conditions, we checked the Picard condition for the three dipole locations with two signals to noise ratios after taking into account the radial orientation of the dipole generator.

The L-curve, GCV curve and the NCPs curve have been plotted. The plots correspond to the three test dipole locations. The next step was to tune the

regularization parameter using the three-parameter choice methods (L-curve, GCV and NCP), we inserted those parameters into the WMNE algorithm to solve the inverse problem. We evaluated the WMNE solution using three measures (Localization error, center of gravity and spatial spreading). Overall, NCP gives the best estimate of the parameter according to the amount of the errors, then GCV and finally the L-curve.

In the second part, another comparative study was conducted. We compared the performance of two popular inverse solvers, sLORETA and eLORETA. In this study, the orientations have been chosen as follows: 30 different orientations selected by 30 points distributed in a uniform way on a unit sphere centered at each dipole location. The regularization parameter was inserted manually in this part. The solutions of both algorithms were evaluated using the same measures (Localization error, center of gravity and spatial spreading). Our results indicate that eLORETA outperform sLORETA on all measures. It produces solution with zero localization error even in the presence of the noise. In contrast, sLORETA did not. These results agree with previous study.

References

- Babiloni F, Babiloni C, Carducci F, Fattorini L, Onorati P, Urbano A. **“Spline Laplacian estimate of EEG potentials over a realistic magnetoc-resonance reconstructed scalp surface model”**, *Electroencephalography and Clinical Neurophysiology*, **98**:363-373, (1996).
- Baillet S, Moshier J, RM L. **“Electromagnetic brain mapping”** *IEEE Signal Processing Magazine*, **18**(6):14–30, (2001).
- B. V., **“Fixed-point iterations in determining the tikhonov regularization parameter”**, *Inverse Problems*, **24**, (2008).
- Cherry S., and Phelps M., **“Imaging brain function with positron emission tomography”**, *Brain Mapping: The Methods*, (1996).
- Dale A. M., Liu A. K., Fischl B. R., Buckner R. L., Belliveau J. W., Lewine J. D., and Holgren E., **“Dynamic statistical parametric neurotechnique mapping: Combining fMRI and MEG for high-resolution imaging of cortical activity”**, *Neuron*, **26**, 55-67(2000).
- Darvas F, Pantazis D, Kucukaltun Yildirim E, Leahy R. **“Mapping human brain function with MEG and EEG: methods and validation. NeuroImage”**, **23**:S289–S299. Darvas (2004).
- D. Krawczyk-Stando and M. Rudnicki, **“The use of l-curve and u-curve in inverse electromagnetic modeling”**, *Intell. Comput. Tech. Appl. Electromagn.*, **119**, 73-82(2008).
- Fender D., Gevins S., and Remonds A., **“Source localization of brain electrical activity methods of analysis of brain electrical and**

- magnetic signals"**, Handbook of electroencephalography and clinical neurophysiology, **1**, 355-403(1987).
- Fender D., "**Source localization of brain electrical activity**", In: Gevins AS, Remond A, editors. Methods of analysis of brain electrical and magnetic signals. Amsterdam, the Netherlands; Elsevier, 355403, (1987).
 - Frank E. "**Electric potential produced by two point current sources in a homogeneous conduction sphere**" Applied Physics; **23**(11):1225–1228, (1952).
 - Golub G., Heath M., and Wahba G., "**Generalized cross-validation as a method for choosing a good ridge parameter**", Technometrics, 215-223(1979).
 - Gorodnitsky I., George J., and Rao B., "**Neuromagnetic source imaging with FOCUSS: a recursive weighted minimum norm algorithm**", Electroencephalography and Clinical Neurophysiology, **95**, 231-251(1995).
 - GrechR., Cassar T., Muscat J., Camilleri K. P., Fabri1 S. G., Zervakis M., Xanthopoulos P.,Sakkalis V., and Vanrumste, B., "**Review on solving the inverse problem in EEG source analysis**",NeuroEngineering and Rehabilitation, **5** (25), 1-33(2008).
 - Hallez H, Vanrumste B, Van Hese P, D'Asseler Y, Lemahieu I, Van de Walle R, "**A finite difference method with reciprocity used to incorporate anisotropy in electroencephalogram dipole source**

- localization**", Phys Med Biol. 2005 Aug 21;50(16):3787-806. Epub (2005).
- Hämäläinen M. S., Hari R., Ilmoniemi R. J., Knuutila J., and Lounasmaa O. V., "**Magnetoencephalography theory, instrumentation, and applications to noninvasive studies of the working human brain**", Rev. Mod. Phys., **65**(12), 413-497(1993).
 - Hämäläinen M., and Ilmoniemi R., "**Interpreting measured magnetic fields of the brain: estimates of current distributions**" Tech. Rep., TKK-F-A559(1984).
 - Hansen P., and O'leary D., "**The use of the l-curve in the regularization of discrete ill-posed problems**", SIAM J. Sci. Comput., **14**, 487-1503(1993).
 - Hansen P., "**Regularization tools: A matlab package for analysis and solution of discrete ill-posed problems**", Numerical Algorithms, **6**, 1-35(1994).
 - Hansen P., Kilmer M., and Kjeldsen R., "**Exploiting residual information in the parameter choice for discrete ill-posed problems**", BIT, **46**, 41-59(2006).
 - Hansen P., and Kilmer M., "**A parameter-choice method that exploits residual information**," PAMM, **7**, 1021705-1021706(2007).
 - Hansen P., "**The l-curve and its use in the numerical treatment of inverse problems**", In Computational Inverse Problems in Electrocardiology Edited by: Johnston P. WIT Press:, 119-142(2001).

- Johnston P., and Gulrajani R., "**A new method for regularization parameter determination in the inverse problem of electrocardiography**", IEEE Trans. Biomed. Eng., **44**, 19-39(1997).
- Johnston P., and Gulrajani R., "**An analysis of the zero-crossing method for choosing regularization parameter**", SIAM J. Sci. Comput., **24**, 428-442(2006).
- KHEMAKHEM R., BEN HAMIDA A., TALEBAHMED R., and DERAMBURE P., "**New hybrid method for the 3d reconstruction of neuronal activity in the brain**", 15th International Conference on Systems, Signals and Image Processing, (2008).
- Klimesch W., "**Memory processes, brain oscillations and EEG synchronization**", International Journal of Psychophysiology (1996).
- Krawczyk-Stando D. and Rudnicki M., "**Regularization parameter selection in discrete ill-posed problems-the use of the u-curve**", Int. J. Appl. Math. Comput. Sci, **17**, 157-164(2007).
- Law SK, Nunez PL, Wijesinghe, R S. "**High resolution EEG using spline generated surface Laplacians on spherical and ellipsoidal surfaces**", IEEE Transactions on Biomedical Engineering, **40**,145-153, (1993).
- Lin F., Witzel T., Ahlfors, S. P., Stufflebeam S., Belliveau J., and M. S. Hämmäläinen, "**Assessing and improving the spatial accuracy in meg source localization by depthweighted minimum-norm estimates**," Journal of NeuroImage, **31**, 160-171(2006).

- Liu A., Belliveau J., and AM. D., "**Spatiotemporal imaging of human brain activity using functional MRI constrained magnetoencephalography data: Monte carlo simulations**", in NatlAcadSci, 8945-50(1998).
- Liu H., Gao X., Schimpf P. H., Yang F., and Gao S., "**A recursive algorithm for the three-dimensional imaging of brain electric activity: Shrinking loreta-focuss**", IEEE TRANSACTIONS ON BIOMEDICAL ENGINEERING, **51**(10), (2004).
- Min W., Luo G., "**Medical Applications of EEG Wave Classification**", Chance **22**(4):14-20, (2009).
- Morozov V., "**On the solution of functional equations by the method of regularization**", Soviet Math. Dokl., 414-417(1966).
- Nunez P L, Silberstein R B, Cadusch P J, Wijesinghe R S, Westdorp A F, Srinivasan R: "**A theoretical and experimental study of high resolution EEG based on surface Laplacians and cortical imaging**", Electroencephalography and Clinical Neurophysiology, **90**, 40-57, (1994).
- Pascual-Marqui R., "**Standardized low resolution brain electromagnetic tomography (sloreta): Technical details**", Methods and Findings in Experimental and Clinical Pharmacology, **24**(5), 22612(2002).
- Pascual-Marqui R., "**Review of methods for solving the EEG inverse problem**", International Journal of Bioelectromagnetism, **1**, 75-86(1999).

- Pascual-Marqui R., Michel C., and Lehmann D., "**Low resolution electromagnetic tomography: a new method for localizing electrical activity in the brain**", International Journal of Psychophysiology, **18**, 49-65(1994).
- Pascual-Marqui R., "**Review of methods for solving the EEG inverse problem**", International Journal of Bioelectromagnetism, **1**, 75-86(1999).
- Pascual-Marqui RD "**Discrete,3D distributed linear imaging methods of electric neuronal activity**". Part 1: exact, zero error localization, arXiv: 0710.3341[math-ph], 2007-October-17 (2007).
- Rubio D., and Troparevsky M. I., "**The EEG forward problem: theoretical and numerical aspects**", Latin American applied research, **36**, 87-92(2006).
- Rush S, Driscoll D. "**current distribution in the brain from surface electrodes**". Anesth. Analg, **47**(6):717–723, (1968).
- Salman A, Malony A, Turovets S, Volkov V, David Ozog D, Don Tucker D. "**Concurrency in electrical neuroinformatics: parallel computation for studying the volume conduction of brain electrical fields in human head tissues**" Concurrency and computation practice and experience, Pages 2213–2236, (2014).
- Salman A, Turovets S, Malony A, Poolman P, Davey C, Eriksen J, Tucker D. "**Noninvasive conductivity extraction for high-resolution EEG source localization**". Advances in Clinical Neuroscience and Rehabilitation 2006; **6**:27–28.

- S. M. and von Cramon D., "**Two bilateral sources of the late aep as identified by a spatio-temporal dipole model**", *ElectroencephClinNeurophysiol*, **62**, 32-44(1985).
- Schimpf P., Liu H., Haueisen J., and Ramon C., "**Balancing resolution and localization performance with a modified sloreta / focuss algorithm**", In 14th International Conference on Biomagnetism, (2004).
- Sidman R D, "A method for simulating intracerebral potential fields: the cortical imaging method", *Journal of Clinical Neurophysiology*, (**8**)432-441, (1991).
- Srinivasan R, Murias M, Tucker D M, "**Estimates of the spatial Nyquist of EEG**", *Behavior Research Methods, Instruments, and Computers* , **30**, 8-19, (1998b).
- Srinivasan R., "**Cognitive neuroscience of creativity: EEG based approaches**", *Methods*, **42**(1):109-16, (2007).
- Tarantola, "**Inverse Problem Theory and Methods for Model Parameter Estimation**", *Society for Industrial and Applied Mathematics*, (2005).
- Tikhonov A., "**Solution of incorrectly formulated problems and the regularization method**", *Soviet Math. Dokl.*,**4**, 1035-1038(1963).
- Tucker D., "**Spatial sampling of head electrical _elds: the geodesic sensor net**", *Electroencephalography and Clinical Neurophysiology*, **87**,154-163(1993).

- Tudor, M., L. Tudor, and K. I. Tudor. "**Hans Berger (1873-1941)--the History of Electroencephalography**" *Acta Med Croatica*, **59**(4): 307-313 (2005).
- Uitert R., Weinstein D., and Johnson C., "**Volume currents in forward and inverse magnetoencephalographic simulations using realistic head models**", *Ann. Biomed. Eng.*,**31**, 21-31(2003).
- Ventouras E., Papageorgiou C., Uzunoglu N., and Christodoulou G., "**Tikhonov regularization using a minimum-product criterion: Application to brain electrical tomography**", *Proceedings of the 23rd Annual Conference, IEEE*, **1**, (2001).
- Wahba G., "**Practical approximate solutions to linear operator equations when the data are noisy**", *SIAM J. Numer. Anal.*, 651-667(1977).
- Wegman E. and Martinez Y. E., "**Parameter selection for constrained solutions to ill-posed problems**", *Computing Science and Statistics*,**32**, 333-347(2000).

Appendix A

Localization errors, Errors using center of gravity and Spatial spreading errors have been shown in the tables below. The errors are shown after inserting the estimated regularization parameter from the three methods (L-curve, NCP and GCV). WMNE is the used inverse problem solver.

1- Using shallow dipole to generate the synthetic EEG data:

Table A.1: Localization errors using WMNE algorithm after substituting the regularization parameter from the three methods (L-curve, NCP and GCV). Shallow dipole is used to generate the synthetic data.

SNR	Localization error (mm)		
	L-curve	GCV	NCP
2	45.734	37.345	37.419
4	41.904	36.456	32.387
6	37.335	33.214	32.439
8	33.456	29.871	27.399
10	30.434	25.234	25.473
12	27.345	20.243	20.484
14	22.343	20.280	19.494

Table A.2: Errors using COG measure, after substituting the regularization parameter from the three methods (L-curve, NCP and GCV). Shallow dipole is used to generate the synthetic data.

SNR	Errors using Center of gravity measure		
	L-curve	GCV	NCP
2	29.736	27.345	29.219
4	24.904	22.456	23.389
6	22.363	20.215	22.494
8	23.456	18.872	17.393
10	20.423	16.234	15.433
12	19.345	16.244	16.444
14	19.314	14.282	15.447

Table A.3: Errors using Spatial Spreading measure, after substituting the regularization parameter from the three methods (L-curve, NCP and GCV). Shallow dipole is used to generate the synthetic data.

SNR	Spatial Spreading Errors		
	L-curve	GCV	NCP
2	70.734	66.345	64.419
4	67.904	62.456	63.387
6	66.333	61.214	60.439
8	62.456	53.871	51.399
10	55.432	45.234	45.473
12	53.345	47.243	48.484
14	50.341	46.280	38.494

2- Using dipole at the middle to generate the synthetic EEG data:

Table A.4: Localization errors using WMNE algorithm after substituting the regularization parameter from the three methods (L-curve, NCP and GCV). Mid dipole is used to generate the synthetic data.

SNR	Localization error(mm)		
	L-curve	GCV	NCP
2	53.716	45.345	40.419
4	51.904	36.452	32.387
6	44.332	34.214	32.439
8	43.456	29.871	29.399
10	35.431	27.232	27.473
12	27.345	25.243	22.484
14	25.343	23.280	19.494

Table A.5: Errors using COG measure, after substituting the regularization parameter from the three methods (L-curve, NCP and GCV). Mid dipole is used to generate the synthetic data.

SNR	Errors using Center of gravity measure		
	L-curve	GCV	NCP
2	35.73416	29.345	31.419
4	34.904	25.456	26.38789
6	31.33	20.2145	22.4394
8	27.456	18.8712	23.3993
10	25.43	18.234	19.4733
12	23.345	16.2434	16.4844
14	20.34	15.2802	14.4947

Table A.6: Errors using Spatial Spreading measure, after substituting the regularization parameter from the three methods (L-curve, NCP and GCV). Mid dipole is used to generate the synthetic data.

SNR	Spatial spreading errors		
	L-curve	GCV	NCP
2	75.734	69.345	65.419
4	70.904	66.456	63.387
6	66.332	61.214	62.439
8	66.456	56.871	54.399
10	63.431	50.233	45.473
12	61.345	47.243	43.484
14	63.343	49.280	38.494

3- Using deep located dipole to generate the synthetic EEG data:

Table A.7: Localization errors, after substituting the regularization parameter from the three methods (L-curve, NCP and GCV). Deep dipole is used to generate the synthetic data.

SNR	Localization errors		
	L-curve	GCV	NCP
2	61.73416	48.345	46.419
4	57.904	39.456	35.38789
6	56.33	37.2145	32.4394
8	44.456	29.8712	29.3993
10	33.43	27.234	28.4733
12	35.345	26.2434	22.4844
14	25.34	18.2802	19.4947

Table A.8: Errors using COG measure, after substituting the regularization parameter from the three methods (L-curve, NCP and GCV). Deep dipole is used to generate the synthetic data.

SNR	Errors using Center of gravity measure		
	L-curve	GCV	NCP
2	39.734	29.745	31.419
4	34.504	26.456	28.387
6	33.332	23.214	22.339
8	30.456	20.871	24.399
10	27.434	18.634	19.073
12	23.945	16.293	16.684
14	22.345	19.280	18.494

Table A.9: Errors using Spatial Spreading measure, after substituting the regularization parameter from the three methods (L-curve, NCP and GCV). Deep dipole is used to generate the synthetic data.

SNR	Spatial Spreading Errors		
	L-curve	GCV	NCP
2	79.734	69.345	67.419
4	72.904	65.456	63.387
6	66.332	63.214	63.439
8	64.456	58.871	56.399
10	61.431	56.234	48.473
12	61.345	49.243	45.484
14	58.344	47.280	43.494

Appendix B

Localization errors, errors using center of gravity and Spatial spreading errors have been shown in the tables below, using two algorithms for solving the inverse problem (eLORETA and sLORETA). Mid dipole is used to generate the synthetic EEG data.

Table B.1: Localization errors of eLORETA and sLORETA algorithms.

SNR	Localization errors	
	eLORETA	sLORETA
2	10.419	16.286
4	8.387	13.256
6	5.439	10.267
8	3.399	8.265
10	0	7.236
12	0	6.852
14	0	6.284

Table B.2: Errors using COG measure of eLORETA and sLORETA algorithms.

SNR	Errors using Center of gravity measure	
	eLORETA	sLORETA
2	9.387	26.976
4	8.893	18.665
6	6.214	15.652
8	5.871	13.723
10	4.234	10.235
12	1.243	7.236
14	0.000	4.325

Table B.3: Spatial Spreading errors of eLORETA and sLORETA algorithms.

SNR	Spatial Spreading errors	
	eLORETA	sLORETA
2	40.233	47.343
4	42.349	46.326
6	39.234	45.562
8	35.099	43.765
10	32.390	40.215
12	29.382	38.215
14	25.920	35.254

جامعة النجاح الوطنية

كلية الدراسات العليا

دراسة مقارنة لطرق تقدير معامل التسوية في مسألة تخطيط كهربية الدماغ المعاكسة

إعداد

محمد جميل ابوريدي

إشراف

د. عدنان سلمان

قدمت هذه الأطروحة استكمالاً لمتطلبات الحصول على درجة الماجستير في الحوسبة المتقدمة
بكلية الدراسات العليا في جامعة النجاح الوطنية في نابلس، فلسطين.

2016

ب

دراسة مقارنة لطرق تقدير معامل التسوية في مسألة تخطيط كهربية الدماغ المعاكسة

إعداد

محمد جميل ابوريدي

إشراف

د.عدنان سلمان

الملخص

التحقيق في نشاط الخلايا العصبية في دماغ الانسان يعتمد على ربط اشارات جهاز EEG بالنسبة الى المصدر المولد لها في قشرة الدماغ، والذي يتطلب حل المسألة العكسية لايجاد المصدر. هذه المسألة تحتوي على مشكلتين: الاولى انها ill condition والثانية انها under determinate، لذلك تعتبر ill posed. لايجاد حل لمثل هذا النوع من المسائل، يجب تطبيق التسوية. تكمن الصعوبة في تطبيق التسوية في اختيار معاملها المثالي. معامل التسوية المثالي يكون بحيث يوازي كمية التسوية المضافة والحد الاصلي من المسألة العكسية.

العديد من الطرق وضعت لايجاد معامل التسوية المثالي لهذا النوع من المسائل، في هذه الاطروحة قمنا بتطبيق ثلاثة طرق لايجاد معامل التسوية في المسألة العكسية لايجاد مصدر اشارات ال EEG. وهي (L-curve ،GCV ،NCP). ومن ثم قمنا بمقارنة اداء هذه الطرق من حيث الدقة والموثوقية. واخترنا خوارزمية WMNE لحل المسألة العكسية مع اضافة العديد من مستويات الضجيج الى مولدات الاشارة المختلفة التي تم محاكاتها. الحل الامامي والذي من خلاله يتم ايجاد الجهد الكهربائي الناتج من كل مصدر على الرأس تم حسابه من خلال FDM. نتائج هذه الدراسة اشارت الى ان طريقة NCP اعطت افضل تقدير لمعامل التسوية بشكل عام. عند بعض مستويات الضجيج اعطت طريقة GCV نتائج مشابهة لطريقة NCP، على النقيض من L-curve التي اعطت اعلى نسبة خطأ.

علاوة على ذلك، تم مقارنة اداء خوارزمتان لحل المسألة العكسية وهما LORETA وeLORETA. أشارت النتائج الى أن eLORETA اعطت افضل نتائج من حيث نسبة الخطأ.

